

**UC Davis**

**UC Davis Electronic Theses and Dissertations**

**Title**

A High-Resolution Oxygen Analyzer and Other Tools for Plant Nutrition Research and Beyond

**Permalink**

<https://escholarship.org/uc/item/4t93f2wc>

**Author**

Knapp, Anna

**Publication Date**

2024

Peer reviewed|Thesis/dissertation

A High-Resolution Oxygen Analyzer and Other Tools for Plant Nutrition Research and Beyond

By

ANNA KNAPP  
DISSERTATION

Submitted in partial satisfaction of the requirements for the degree of

DOCTOR OF PHILOSOPHY

in

Horticulture and Agronomy

in the

OFFICE OF GRADUATE STUDIES

of the

UNIVERSITY OF CALIFORNIA

DAVIS

Approved:

---

Arnold Bloom, Chair

---

Troy Magney

---

Stavros Vougioukas

Committee in Charge

2024

## Acknowledgments

First and foremost, I want to thank my major professor Arnold Bloom who made all of this work possible. I am extremely grateful for his encouragement and mentorship throughout my doctoral program.

I am grateful the other members of the Bloom lab and our collaborators who provided indispensable assistance. In particular, I want to thank Jordan Stefani and Ella Katz who I worked closely with on the rosette area measurement tool.

I am grateful for my family and friends who have supported me along the way; my parents for inspiring my love of learning and of the natural world and my sister for always encouraging my academic pursuits.

Finally, I am forever grateful to my husband for the immeasurable support he has given me throughout this endeavor.

## Abstract

The steady increase in atmospheric CO<sub>2</sub> since the industrial revolution is well established as the major driver of global climate change but its direct impacts on biochemical processes like photosynthesis are also of major concern. Some crop plant species have been shown to be less effective at assimilating nitrate, the most abundant form of nitrogen available to plants in most agricultural soils, when grown under elevated CO<sub>2</sub>. This indicates that rising CO<sub>2</sub> concentrations could negatively impact the nitrogen use efficiency of many important crop species and may explain why protein content in some plant species decreases with CO<sub>2</sub> enrichment. Improved techniques to measure nitrogen metabolism in plants are needed to further study the underlying cause of this phenomenon and mitigate the impact of rising atmospheric CO<sub>2</sub> on our food supply. The three projects described here are a part of this effort.

Chapter 1 describes a rosette area measurement tool that was developed as part of a larger study investigating the genetic basis of plant response to different nitrogen forms and concentrations. This tool was able to accurately estimate rosette area from photographs of *Arabidopsis* seedlings grown on agar plates even when the photographs did not provide a scale.

We present a general-purpose ultra-high-resolution data acquisition system in chapter 2. The system interfaces a 32-bit analog to digital converter with a Raspberry Pi single board computer. We provide a simple open-source hardware design and easy to use software libraries enabling this system to be easily built and adapted for any purpose. Finally, we demonstrate the high performance of the system by making precise temperature measurements. Many elements of this data acquisition system were used in the Oxygen analyzer described in chapter 3.

Chapter 3 documents the design and characterization of a novel high-resolution oxygen analyzer designed to measure small O<sub>2</sub> fluxes against the large ambient background. The original motivation for this instrument was to estimate nitrate assimilation in plants through the ratio of CO<sub>2</sub> assimilated to O<sub>2</sub> evolved. The design is based around a zirconia O<sub>2</sub> sensor that has not traditionally been used for high precision applications. The O<sub>2</sub> measurement repeatability of the analyzer was better than 70 ppm, nearly 2 orders of magnitude better than what had previously been reported for an analyzer using this type of sensor. Further improvements to temperature control may yield even higher precision enabling measurements of photosynthetic O<sub>2</sub> fluxes.

## Table of Contents

<b>Title</b>	i
<b>Acknowledgments</b>	ii
<b>Abstract</b>	iii
<b>Table of contents</b>	v
<b>Introduction</b>	1
Rising CO <sub>2</sub> and nitrogen nutrition	1
Nitrate assimilation and ammonium tolerance	2
Simultaneous O <sub>2</sub> and CO <sub>2</sub> measurement	3
<b>Chapter 1 - Novel method for the quantification of rosette area from images of <i>Arabidopsis</i> seedlings grown on agar plates</b>	8
<b>Chapter 2 - Easy as piads: A low-cost, ultra-high-resolution data acquisition system using a Raspberry Pi</b>	16
<b>Chapter 3 - A high-resolution oxygen analyzer using a zirconia sensor</b>	23
<b>Conclusion and future directions</b>	37
<b>Appendix - Detailed oxygen analyzer design description and supplemental figures</b>	40

## Introduction

### **Rising CO<sub>2</sub> and nitrogen nutrition:**

Humans began burning fossil fuels in large quantities around 300 years ago and as a result, the carbon dioxide concentration in the atmosphere has risen from 275 ppm to around 420 ppm - more than a 50% increase (Keeling et al., 2017). Rising atmospheric CO<sub>2</sub> and the associated global warming has profound impacts on plants and agriculture. Extreme temperature and precipitation changes are projected to reduce the yields of many commodity and specialty crops (Gowda et al., 2018). The atmospheric CO<sub>2</sub> concentration itself also directly affects plants but how this will impact crop yields is still controversial.

One prediction is that elevated CO<sub>2</sub> will stimulate photosynthesis and have a net “fertilization” effect on global vegetation, increasing gross primary productivity (Schimel et al., 2014). Elevated CO<sub>2</sub> concentrations also decrease stomatal conductance because relatively less exchange with the atmosphere is required to achieve sufficient carbon fixation. Reduced stomatal conductance may partially counteract water stress caused by climate change related drought and higher temperatures (Swann et al., 2016). Flux tower measurements and satellite observations in recent decades have shown increases in forest net ecosystem productivity (Fernández-Martínez et al., 2017) and leaf area index (Zhu et al., 2016) supporting the CO<sub>2</sub>-fertilization effect hypotheses. On the other hand, some observational studies have shown any fertilization effects may be short-lived as the relative increase in productivity per unit CO<sub>2</sub> concentration decreases over time (Peñuelas et al., 2017, Wang et al., 2020).

Nitrogen availability is implicated as a major limiting factor in plant's response to elevated CO<sub>2</sub>. In long term CO<sub>2</sub> enrichment experiments nitrogen limitation has been found to significantly reduce CO<sub>2</sub> fertilization effects (Reich et al., 2006, Norby et al., 2010). Moreover, atmospheric CO<sub>2</sub> concentration and crop nutritional quality are inversely related: protein content declines in C<sub>3</sub> crops grown under elevated CO<sub>2</sub> vs. those grown in ambient CO<sub>2</sub> (Taub et al., 2008). This finding further supports a link between nitrogen limitation and elevated CO<sub>2</sub> and has important implications for the future of human and animal nutrition because C<sub>3</sub> crops like wheat are an important protein source globally (Shiferaw et al., 2013, White et al., 2022).

#### **Nitrate assimilation and ammonium tolerance:**

Elevated CO<sub>2</sub> has been shown in multiple studies to inhibit nitrate assimilation in C<sub>3</sub> crops (Bloom et al., 2010, 2012) which would, at least in part, explain the decline in protein under elevated CO<sub>2</sub> and the nitrogen dependence of the CO<sub>2</sub> fertilization effect. Nitrate is the most abundant form of nitrogen in most agricultural soils and in many global ecosystems (Miller et al., 2004) making plants' ability to effectively utilize this form of nitrogen especially important.

The mechanisms of nitrate assimilation inhibition by CO<sub>2</sub> are not yet fully understood but one promising hypothesis is that C<sub>3</sub> plants are able to use some of the energy which was traditionally thought to be dissipated as heat during photorespiration and use it for the reduction of nitrate to nitrite (Bloom, 2014, Shi & Bloom, 2021). Reducing nitrate to a usable form during nitrate assimilation is a very energetically expensive process, which is one of the reasons nitrate is so abundant in agricultural soils. By harnessing energy from photorespiration, which has previously been considered wasteful, plants may more easily access a reservoir of soil nitrogen that is untapped by other organisms.

Further research is needed to find strategies to mitigate the impact of rising atmospheric CO<sub>2</sub> on our food supply, but one possible strategy under investigation is to provide other forms of nitrogen. Ammonium and other reduced forms of nitrogen are much less energetically expensive for plants to assimilate, and the rate of assimilation for these compounds is not inhibited by elevated CO<sub>2</sub>. Providing C<sub>3</sub> crops like wheat with more ammonium could help prevent protein decline under elevated CO<sub>2</sub> but ammonium has two major issues that need to be addressed: nitrification and ammonium toxicity. Most fertilizers applied to crops contain ammonia but soil nitrifiers quickly oxidize this form of nitrogen into nitrate. Farmers often apply synthetic nitrification inhibitors alongside fertilizers in an attempt to slow this process. More recently, the root exudates of some important crop species have been found to contain biological nitrification inhibitors (Coskun et al., 2017). Even if these compounds can effectively inhibit nitrification in agricultural soils, crops would still have to contend with toxicity from ammonium accumulation. Ammonium is highly toxic to plants whereas nitrate has relatively low toxicity. The mechanisms behind ammonium toxicity are not yet fully understood and neither are those behind ammonium tolerance (Esteban et al., 2016). There is great natural variation in plants' tolerance to ammonium, even among varieties within the same species (Sarasketa et al., 2014, Katz et al., 2022). Ammonium tolerance can, therefore, be treated as a beneficial crop trait and selected for in breeding programs.

### **Simultaneous Measurement of O<sub>2</sub> and CO<sub>2</sub>**

Measuring nitrate assimilation in plants can be used to study variation in their responses to elevated CO<sub>2</sub> as well as quantify the relative utilization of ammonium vs nitrate. Various methods have been used to quantify nitrate assimilation but one of particular interest is

Assimilatory Quotient (AQ) which refers to the ratio of CO<sub>2</sub> consumed to O<sub>2</sub> evolved during photosynthesis (Bloom et al., 1989). AQ measurements are able to estimate nitrate assimilation because plants have coupled this energetically expensive reaction with photosynthesis. During photosynthesis, reduced ferredoxin generated during the light-dependent reactions can either provide reducing power to the CBB cycle (carbon fixation) or to nitrite reductase (nitrate assimilation) (Hawkesford et al., 2023). When plants are assimilating nitrate, some of the reduced ferredoxin generated from the oxygen-evolving step of photosynthesis goes towards nitrate assimilation rather than carbon fixation, thereby lowering the amount of CO<sub>2</sub> fixed per O<sub>2</sub> evolved - in other words, lowering the AQ.

AQ measurements have the advantage of allowing for non-destructive real-time estimation of nitrate assimilation in living plants but are not widely used due to the difficulty of measuring very small O<sub>2</sub> fluxes against the large ambient background concentration of 20.9%. Currently there are no commercially available O<sub>2</sub> analyzers with a high enough precision for measuring AQ. AQ measurement in previous studies has either been done with room-sized custom-built O<sub>2</sub> analyzers (Bloom et al., 1989) or with commercial analyzers that have since been discontinued (LI-COR Biosciences, 2022) indicating a need for new instrumentation development.

The following three chapters describe different tools that were developed for research needs related to investigating the impacts of rising CO<sub>2</sub> on crop nutrition, but many have additional applications beyond their original purpose. The first chapter describes an image analysis tool that was originally developed to measure the rosette area of *Arabidopsis* seedlings grown on agar plates as part of a larger study investigating the genetic basis of plant response to nitrogen form and concentration. The second two chapters describe a novel high precision O<sub>2</sub>

analyzer that was initially developed to measure AQ and a related general purpose data acquisition system that was developed alongside the O<sub>2</sub> analyzer.

## References

- Bloom, A. J. (2014). Photorespiration and nitrate assimilation: A major intersection between plant carbon and nitrogen. *Photosynthesis Research*, *123*(2), 117–128. <https://doi.org/10.1007/s11120-014-0056-y>
- Bloom, A. J., Asensio, J. S., Randall, L., Rachmilevitch, S., Cousins, A. B., & Carlisle, E. A. (2012). CO<sub>2</sub> enrichment inhibits shoot nitrate assimilation in C<sub>3</sub> but not C<sub>4</sub> plants and slows growth under nitrate in C<sub>3</sub> plants. *Ecology*, *93*(2), 355–367. <https://doi.org/10.1890/11-0485.1>
- Bloom, A. J., Burger, M., Asensio, J. S., & Cousins, A. B. (2010). Carbon dioxide enrichment inhibits nitrate assimilation in wheat and *Arabidopsis*. *Science*, *328*(5980), 899–903. <https://doi.org/10.1126/science.1186440>
- Bloom, A. J., Caldwell, R. M., Finazzo, J., Warner, R. L., & Weissbart, J. (1989). Oxygen and carbon dioxide fluxes from barley shoots depend on nitrate assimilation. *Plant Physiology*, *91*(1), 352–356. <https://doi.org/10.1104/pp.91.1.352>
- Coskun, D., Britto, D. T., Shi, W., & Kronzucker, H. J. (2017). Nitrogen transformations in modern agriculture and the role of biological nitrification inhibition. *Nature Plants*, *3*(6). <https://doi.org/10.1038/nplants.2017.74>
- Esteban, R., Ariz, I., Cruz, C., & Moran, J. F. (2016). Review: Mechanisms of ammonium toxicity and the quest for tolerance. *Plant Science*, *248*, 92–101. <https://doi.org/10.1016/j.plantsci.2016.04.008>
- Fernández-Martínez, M., Vicca, S., Janssens, I. A., Ciais, P., Obersteiner, M., Bartrons, M., Sardans, J., Verger, A., Canadell, J. G., Chevallier, F., Wang, X., Bernhofer, C., Curtis, P. S., Gianelle, D., Grünwald, T., Heinesch, B., Ibrom, A., Knohl, A., Laurila, T., ... Peñuelas, J. (2017). Atmospheric deposition, CO<sub>2</sub>, and change in the Land Carbon Sink. *Scientific Reports*, *7*(1). <https://doi.org/10.1038/s41598-017-08755-8>
- Gowda, P. H., Steiner, J., Olson, C., Boggess, M., Farrigan, T., & Grusak, M. A. (2018). *Chapter 10 : Agriculture and Rural Communities. Impacts, Risks, and Adaptation in the United States: The Fourth National Climate Assessment, Volume II*. <https://doi.org/10.7930/nca4.2018.ch10>
- Hawkesford, M. J., Cakmak, I., Coskun, D., De Kok, L. J., Lambers, H., Schjoerring, J. K., & White, P. J. (2023). Functions of macronutrients. *Marschner's Mineral Nutrition of Plants*, 201–281. <https://doi.org/10.1016/b978-0-12-819773-8.00019-8>
- Katz, E., Knapp, A., Lensink, M., Keller, C. K., Stefani, J., Li, J.-J., Shane, E., Tuermer-Lee, K., Bloom, A. J., & Kliebenstein, D. J. (2022). Genetic variation underlying differential ammonium

and nitrate responses in *Arabidopsis thaliana*. *The Plant Cell*, 34(12), 4696–4713.  
<https://doi.org/10.1093/plcell/koac279>

Keeling, R. F., Keeling, C. D., (2017). Atmospheric Monthly In Situ CO<sub>2</sub> Data - Mauna Loa Observatory, Hawaii (Archive 2024-01-08). In Scripps CO<sub>2</sub> Program Data. UC San Diego Library Digital Collections. <https://doi.org/10.6075/J08W3BHW>

LI-COR Biosciences. (2022) Leaf-level O<sub>2</sub> and CO<sub>2</sub> measurements with the LI-6800 and Picarro G2207-i.

Miller, A. J., & Cramer, M. D. (2005). Root nitrogen acquisition and assimilation. *Plant and Soil*, 274(1–2), 1–36. <https://doi.org/10.1007/s11104-004-0965-1>

Norby, R. J., Warren, J. M., Iversen, C. M., Medlyn, B. E., & McMurtrie, R. E. (2010). CO<sub>2</sub> enhancement of forest productivity constrained by limited nitrogen availability. *Proceedings of the National Academy of Sciences*, 107(45), 19368–19373.  
<https://doi.org/10.1073/pnas.1006463107>

Peñuelas, J., Ciais, P., Canadell, J. G., Janssens, I. A., Fernández-Martínez, M., Carnicer, J., Obersteiner, M., Piao, S., Vautard, R., & Sardans, J. (2017). Shifting from a fertilization-dominated to a warming-dominated period. *Nature Ecology & Evolution*, 1(10), 1438–1445. <https://doi.org/10.1038/s41559-017-0274-8>

Reich, P. B., Hobbie, S. E., Lee, T., Ellsworth, D. S., West, J. B., Tilman, D., Knops, J. M., Naeem, S., & Trost, J. (2006). Nitrogen limitation constrains sustainability of ecosystem response to CO<sub>2</sub>. *Nature*, 440(7086), 922–925. <https://doi.org/10.1038/nature04486>

Sarasketa, A., Gonzalez-Moro, M. B., Gonzalez-Murua, C., & Marino, D. (2014). Exploring ammonium tolerance in a large panel of *Arabidopsis thaliana* natural accessions. *Journal of Experimental Botany*, 65(20), 6023–6033. <https://doi.org/10.1093/jxb/eru342>

Schimel, D., Stephens, B. B., & Fisher, J. B. (2014). Effect of increasing CO<sub>2</sub> on the terrestrial carbon cycle. *Proceedings of the National Academy of Sciences*, 112(2), 436–441.  
<https://doi.org/10.1073/pnas.1407302112>

Shi, X., & Bloom, A. (2021). Photorespiration: The futile cycle? *Plants*, 10(5), 908.  
<https://doi.org/10.3390/plants10050908>

Shiferaw, B., Smale, M., Braun, H.-J., Duveiller, E., Reynolds, M., & Muricho, G. (2013). Crops that feed the world 10. Past successes and future challenges to the role played by wheat in Global Food Security. *Food Security*, 5(3), 291–317. <https://doi.org/10.1007/s12571-013-0263-y>

Swann, A. L., Hoffman, F. M., Koven, C. D., & Randerson, J. T. (2016). Plant responses to increasing CO<sub>2</sub> reduce estimates of climate impacts on drought severity. *Proceedings of the National Academy of Sciences*, 113(36), 10019–10024. <https://doi.org/10.1073/pnas.1604581113>

Taub, D. R., Miller, B., & Allen, H. (2007). Effects of elevated cO<sub>2</sub> on the protein concentration of food crops: A meta-analysis. *Global Change Biology*, 14(3), 565–575.  
<https://doi.org/10.1111/j.1365-2486.2007.01511.x>

Wang, S., Zhang, Y., Ju, W., Chen, J. M., Ciais, P., Cescatti, A., Sardans, J., Janssens, I. A., Wu, M., Berry, J. A., Campbell, E., Fernández-Martínez, M., Alkama, R., Sitch, S., Friedlingstein, P., Smith, W. K., Yuan, W., He, W., Lombardozzi, D., ... Peñuelas, J. (2020). Recent global decline of CO<sub>2</sub> fertilization effects on vegetation photosynthesis. *Science*, *370*(6522), 1295–1300.

<https://doi.org/10.1126/science.abb7772>

White, R. R., & Gleason, C. B. (2022). Global human-edible nutrient supplies, their sources, and correlations with agricultural environmental impact. *Scientific Reports*, *12*(1).

<https://doi.org/10.1038/s41598-022-21135-1>

Zhu, Z., Piao, S., Myneni, R. B., Huang, M., Zeng, Z., Canadell, J. G., Ciais, P., Sitch, S., Friedlingstein, P., Arneeth, A., Cao, C., Cheng, L., Kato, E., Koven, C., Li, Y., Lian, X., Liu, Y., Liu, R., Mao, J., ... Zeng, N. (2016). Greening of the Earth and its drivers. *Nature Climate Change*, *6*(8), 791–795. <https://doi.org/10.1038/nclimate3004>

## Chapter 1

### **Novel method for the quantification of rosette area from images of *Arabidopsis* seedlings grown on agar plates**

*(Applications in Plant Sciences, Vol 10, Issue 6. e11504)*

Anna Knapp<sup>1\*</sup>, Jordan Stefani<sup>1</sup>, Ella Katz<sup>1</sup>, Arnold J. Bloom<sup>1</sup>

<sup>1</sup>Department of Plant Sciences University of California Davis, One Shields Ave. Davis California 95616 USA.

\*Corresponding author

Author Contribution statement:

J.S. and A.K. wrote the software and performed the validation under supervision from E.K. and A.J.B. E.K. provided resources required to validate this method. A.K. prepared the original draft, and A.J.B and E.K. edited and revised it. All authors approved the final version of the manuscript.

# Novel method for the quantification of rosette area from images of *Arabidopsis* seedlings grown on agar plates

Anna Knapp  | Jordan Stefani  | Ella Katz  | Arnold J. Bloom 

Department of Plant Sciences, University of California, Davis, One Shields Ave., Davis, California 95616, USA

## Correspondence

Anna Knapp, Department of Plant Sciences, University of California, Davis, One Shields Ave., Davis, California 95616, USA.  
Email: [aknapp@ucdavis.edu](mailto:aknapp@ucdavis.edu)

## Abstract

**Premise:** The agar-based culture of *Arabidopsis* seedlings is widely used for quantifying root traits. Shoot traits are generally overlooked in these studies, probably because the rosettes are often askew. A technique to assess the shoot surface area of seedlings grown inside agar culture dishes would facilitate simultaneous root and shoot phenotyping.

**Methods:** We developed an image processing workflow in Python that estimates rosette area of *Arabidopsis* seedlings on agar culture dishes. We validated this method by comparing its output with other metrics of seedling growth. As part of a larger study on genetic variation in plant responses to nitrogen form and concentration, we measured the rosette areas from more than 2000 plate images.

**Results:** The rosette area measured from plate images was strongly correlated with the rosette area measured from directly overhead and moderately correlated with seedling mass. Rosette area in the large image set was significantly influenced by genotype and nitrogen treatment. The broad-sense heritability of leaf area measured using this method was 0.28.

**Discussion:** These results indicated that this approach for estimating rosette area produces accurate shoot phenotype data. It can be used with image sets for which other methods of leaf area quantification prove unsuitable.

## KEYWORDS

automated measurement, diversity panel, high-throughput phenotyping, image analysis, leaf area, Python

Automated image analysis techniques enable the non-destructive phenotyping of large plant diversity panels. The 1001 Genomes Project is one example of such a panel; it comprises 1135 sequenced natural accessions of *Arabidopsis thaliana* (L.) Heynh. sampled from a wide range of environments (1001 Genomes Consortium, 2016). Combining these high-quality genetic resources with high-throughput phenotyping methods enables powerful genome-wide association studies.

One technique for evaluating the developmental traits of such large diversity panels is growing the accessions in agar-filled culture dishes. This allows root traits to be quantified quickly using high-throughput image analysis methods. The plants are not destroyed or contaminated in the process and

can therefore be photographed at different stages of growth. One disadvantage of this approach is that the rosettes are askew, so rosette area is usually not assessed even when the leaves are visible in the photographs. Quantifying both root and shoot characteristics is usually preferable because many plant processes involve both organs; for example, nitrogen acquisition and allocation involves root uptake from the rhizosphere, assimilation into organic forms in both the roots and shoots, and translocation throughout the plant (Bloom, 2015). Studying this process requires precise measurements of both the roots and shoots, which has previously been technically difficult.

Here, we show that leaf area measured from plate images is accurate even when the rosettes are somewhat

Anna Knapp and Jordan Stefani contributed equally to this work.

This is an open access article under the terms of the Creative Commons Attribution License, which permits use, distribution and reproduction in any medium, provided the original work is properly cited.

© 2022 The Authors. *Applications in Plant Sciences* published by Wiley Periodicals LLC on behalf of Botanical Society of America.

*Appl. Plant Sci.* 2022;10:e11504.

<https://doi.org/10.1002/aps3.11504>

[wileyonlinelibrary.com/journal/AppsPlantSci](https://wileyonlinelibrary.com/journal/AppsPlantSci)

1 of 7

askew and can therefore be used for rapidly phenotyping large image sets of *Arabidopsis* seedlings. As part of a larger study to examine the genetic basis of plant adaptation to different nitrogen forms and concentrations in the rhizosphere (Katz et al., 2022), we measured leaf area from more than 2000 images of *Arabidopsis* seedlings on agar plates. Our results demonstrate that this measurement is reproducible and provides a useful metric of shoot growth.

## METHODS

### Image sets for validating the accuracy of rosette area measurements from agar plate images

To determine whether rosette area measurements taken from plate images are sufficient for shoot phenotyping, we compared them to both measurements from images of the rosettes photographed from directly overhead and seedling mass.

To compare the overhead and plate image rosette area measurements, six different natural *Arabidopsis* accessions were planted on agar plates containing a base nutrient solution consisting of 2 mM  $\text{CaCl}_2$ , 2 mM  $\text{KH}_2\text{PO}_4$ , 2 mM  $\text{MgSO}_4$ , 1 mM KCl, 0.75 mM MES, 0.5  $\mu\text{M}$   $\text{CuSO}_4$ , 2  $\mu\text{M}$   $\text{MnSO}_4$ , 25  $\mu\text{M}$   $\text{H}_3\text{BO}_3$ , 42  $\mu\text{M}$  FeNaDTPA, 2  $\mu\text{M}$   $\text{ZnSO}_4$ , 0.5  $\mu\text{M}$   $\text{H}_2\text{MoO}_4$ , and 0.8% (w/v) agar. Different concentrations of sucrose (ranging from 0% to 2%) were added to the base media to ensure that there would be a variety of different-sized seedlings. After planting, the plates were kept at 4°C for four days and then placed into a growth chamber with a 14-h day/10-h night cycle. After 12 days of growth, rosette area of the plants was measured in two ways, first from photographs of the seedlings in the plates and second from a photograph of the rosettes placed upright on paper. All photographs from this image set were taken with a Pixel 3A cellphone camera (Google, Mountain View, California, USA). A total of 58 seedlings were grown and measured this way.

As part of a larger study investigating plant responses to different nitrogen forms and concentrations in the rhizosphere, we quantified the rosette area from plate images and compared it with seedling mass. A total of 148 Col-0 seedlings were grown under 10 different nitrogen conditions with either nitrate or ammonium as the sole nitrogen source at concentrations ranging from 0.05 mM to 5 mM. After 12 days of growth, the plates were photographed and the seedlings, including both roots and shoots, were excised and weighed.

### Image set from the *Arabidopsis* diversity panel study

As another part of the aforementioned study, more than 2000 images of *Arabidopsis* seedlings on agar plates were collected. This image set was generated from an experiment

in which the 1135 natural accessions of the 1001 Genomes Project (1001 Genomes Consortium, 2016) were grown under four different nitrogen conditions: 0.1 mM and 1 mM nitrate using  $\text{KNO}_3$  as the sole nitrogen source and 0.1 mM and 1 mM ammonium using  $\text{NH}_4\text{HCO}_3$  as the sole nitrogen source. The seedlings were grown under long-day conditions (16 h light, 8 h dark). The closed plates were photographed 12 days after planting using an EOS Rebel digital camera fitted with an 18–55 mm EF-S lens (Canon, Tokyo, Japan). The root traits, including primary root length and number of lateral roots, were estimated from the images using RootNav, image analysis software that allows the semiautomated quantification of complex root system architectures (Pound et al., 2013).

### Image analysis with Python

Some of the image sets did not have a red two-dimensional scale present, making them unsuitable for rosette area measurement using existing methods such as Easy Leaf Area (Easlon and Bloom, 2014). We developed our own image processing workflows in Python, which were able to use a scale if it was present or, alternatively, to detect the area of the agar plate to serve as a scale. These workflows use the PlantCV package (Gehan et al., 2017) for most of the image-processing functions.

The general steps in the workflow are (1) cropping the image to the plate region, (2) leaf identification and pixel counting, and (3) scale identification. Cropping the image to the region of interest (ROI) was done to save processing time and eliminate background features that could be mistaken for objects of interest. This was done using binary thresholding or edge detection to separate the agar-filled culture dish from the background (Figure 1). The choice to use edge detection to identify the plate versus binary thresholding was dependent on the image set used. The detection of the agar plate also allows for the rotation of the image if the plate is not correctly aligned within the image.

Leaf identification was performed using binary thresholding and object detection (Figure 2). The specific color channel and threshold value used to identify the leaves varied between the different image sets due to different background and lighting conditions, but as long as the images within a set are taken against the same background and with the same lighting conditions then these values should remain consistent for processing the entire set. For the validation images, the “C” channel of CMYK color space was used to identify the leaves, whereas in the diversity panel image set the “B” channel of  $L^*a^*b^*$  color space was used. To determine the appropriate threshold values for an image set, we used the plot histogram function in PlantCV. This function is used to visualize the range of pixel intensity in the color channel of interest. For image sets with lower contrast, the histogram equalization function was used to make thresholding easier. To simplify leaf identification, an ROI was defined for the top section of the cropped image

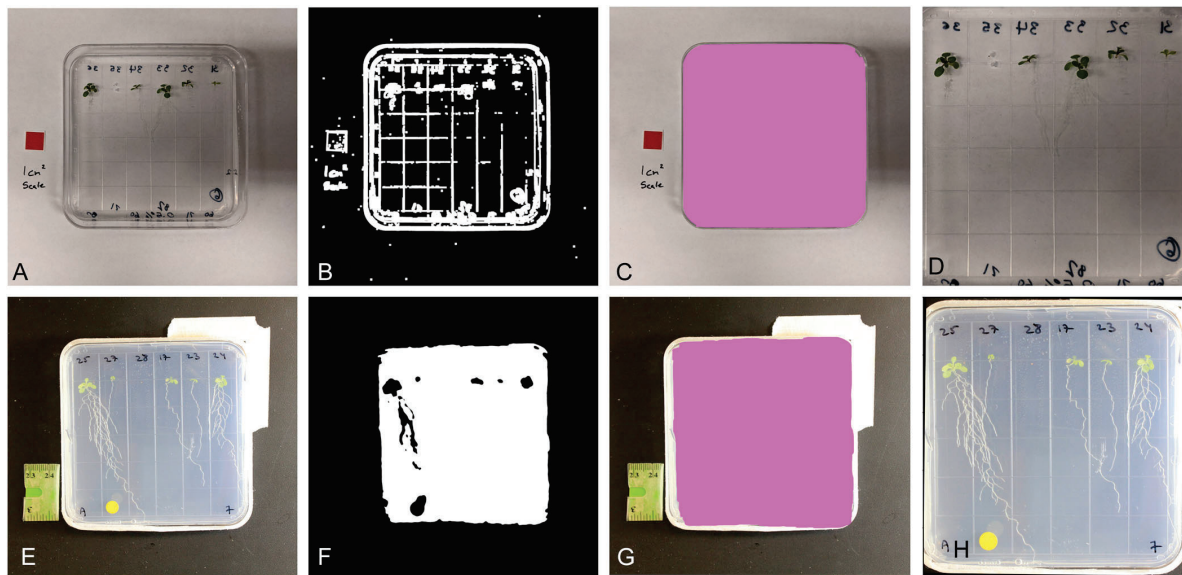


**FIGURE 1** Two different image-processing strategies used to identify the agar plate and automatically crop the image to the plate region. (A–D) Edge detection method. (A) Original image. (B) Binary image generated using canny edge detection. (C) Detection of plate area after the filtering steps. (D) The image after cropping to the plate region. (E–H) Thresholding detection method. (E) Original image. (F) Binary image generated using thresholding. (G) Detection of plate area after the filtering steps. (H) The image after cropping to the plate region and rotating.

where the leaves are found. Objects detected within the ROI were grouped into six shoots using clustering. The image moment of each shoot in the binary image was used to calculate the number of pixels that made up the leaves in each seedling.

Scale identification was performed either by using a reference scale that was placed within the image or using the plate itself as a scale. For dedicated reference scales, the same general process that was used to identify and count pixels of the leaves was used for the scale. Once the number of pixels in the scale or the number of pixels making up the plate were measured, the rosette area could be calculated.

For the large image set of the diversity panel, we automated the workflow in a Python script, which took approximately four hours to process all 2000 images. We were able to estimate rosette area for over 90% of the seedlings that successfully germinated, resulting in 8964 individual measurements. Many of the seedlings that were not measurable had fallen below the middle of the plate and were not within the defined ROI.

The workflows for each image set can be found at <https://github.com/massivejords/Agar-plate-leaf-area> as Jupyter Notebooks (Kluyver et al., 2016), along with the batch analysis Python script used to process the large image set. It is important to note that the parameters used for the various transformations, such as thresholding, grayscale conversion, and scale calculation, are specific to the image set. These parameters would need to be modified when using a different image set, but the general steps would still apply.

## Statistics and data visualization

Linear least-squares regressions were calculated for the validation data sets using Microsoft Excel (Microsoft, Redmond, Washington, USA). R software (R Core Team, 2022) with the RStudio interface (<http://www.rstudio.com/>) and the tidyverse (Wickham et al., 2019) and ggplot2 (Wickham, 2016) packages was used to analyze and visualize the data from the diversity panel study. We performed an ANOVA to test the effect of genotype, nitrogen source, and nitrogen treatment (nitrogen source and concentration) on the seedling rosette area and to determine the broad sense heritability of the trait.

## RESULTS

### Validation

Rosette area measurements taken from plate images and from directly overhead were found to have a strong linear relationship (Figure 3A). Rosette areas from this image set were quantified twice, first using the red square as a scale and then using the plate area as a scale. For each set of measurements, a linear least-squares regression was calculated. The coefficient of determination ( $R^2$ ) for measurements that relied on the red scale was 0.8127, and the slope and  $y$  intercept were 0.875 and  $-1.100$ , respectively. For plate image measurements that used the plate itself as a scale,  $R^2$  was 0.8651, the slope was 0.759, and the  $y$  intercept was  $-0.895$ .

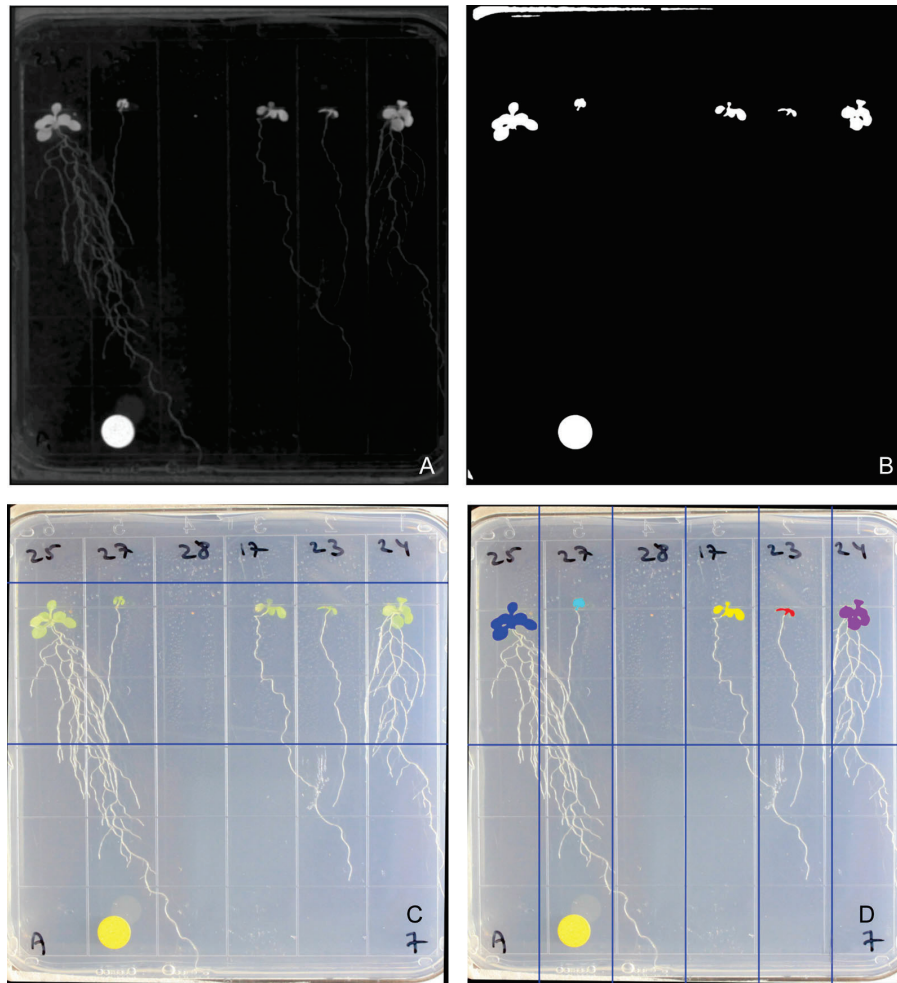


**FIGURE 2** The image-processing steps used for leaf identification. (A) Image converted to black and white using the B channel of the  $L^*a^*b^*$  color space. (B) Binary threshold. (C) Region of interest indicated by the blue lines. (D) Identification of individual shoots using clustering and splitting the image into six sections. Note that one seed failed to germinate so no leaf area was measured.

Seedling mass and rosette area were also found to be positively correlated (Figure 3B), although this correlation was not as strong ( $R^2 = 0.4959$ , slope = 3537.8,  $y$  intercept = 3.5).

### Rosette area response to nitrogen nutrition in an *Arabidopsis* diversity panel

The response of rosette area to the four nitrogen nutrient conditions across the 1135 accessions is shown in Figure 4. Overall, the seedlings grown in 1 mM nitrate had the greatest mean rosette area. Some accessions showed extreme differences in their responses to the nitrogen conditions. Nitrogen source and treatment both had significant effects on rosette area ( $F_{1,5360} = 547.62$ ,  $P < 0.0001$  and  $F_{2,5360} = 238.94$ ,  $P < 0.0001$ , respectively).

Genotype also had a significant effect ( $F_{1020,5360} = 3.70$ ,  $P < 0.0001$ ), and the percentage of the total sum of squares attributed to this factor was used to calculate an  $H^2$  of 0.28. The heritability of primary root length was 0.41.

### DISCUSSION

The strong positive linear relationship between the rosette area measurements taken from the plate images and those taken from photographs of excised rosettes demonstrates that using plate images for shoot trait analyses can yield meaningful phenotype data with minimal effort. While the correlation between rosette area measured from plate images and seedling mass was not as strong, it was still sufficient to indicate that this is a

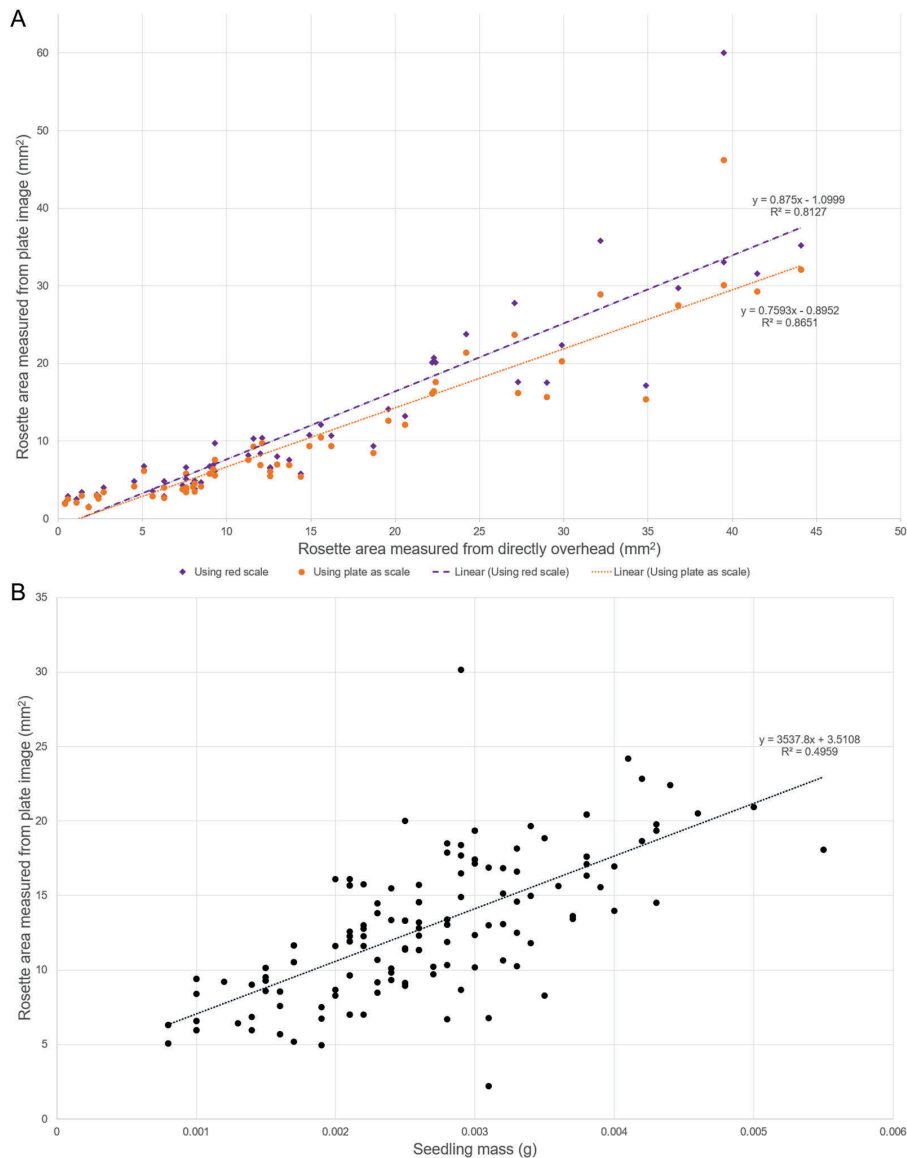


**FIGURE 3** Scatterplots of rosette area measured from agar plate images compared with other metrics of growth. Dashed lines indicate linear least-squares regression fits to the data points. (A) Scatterplot comparing *Arabidopsis* seedling rosette areas measured from agar plates or directly overhead. (B) *Arabidopsis* seedling rosette area measured from agar plates compared with seedling mass.

viable method for estimating plant growth. A lower correlation between these measurements is also to be expected because the seedling mass includes both shoot and root mass and is therefore not as specific to shoot growth as is the rosette area.

We were also able to apply this analysis to an image set generated for the purpose of root phenotyping, allowing us to obtain additional valuable phenotypic information. The rosette area measured using this technique across a large *Arabidopsis* diversity panel was found to be heritable and

showed a significant response to rhizosphere nitrogen form and concentration. These results were in line with other developmental traits measured using established techniques, such as primary root length measured using RootNav (Pound et al., 2013).

Agar plate images are widely used for the non-destructive measurement of *Arabidopsis* root traits. Here, we showed that useful shoot trait information can also be collected from these same images, enabling simultaneous root and shoot phenotyping. This can be done quickly

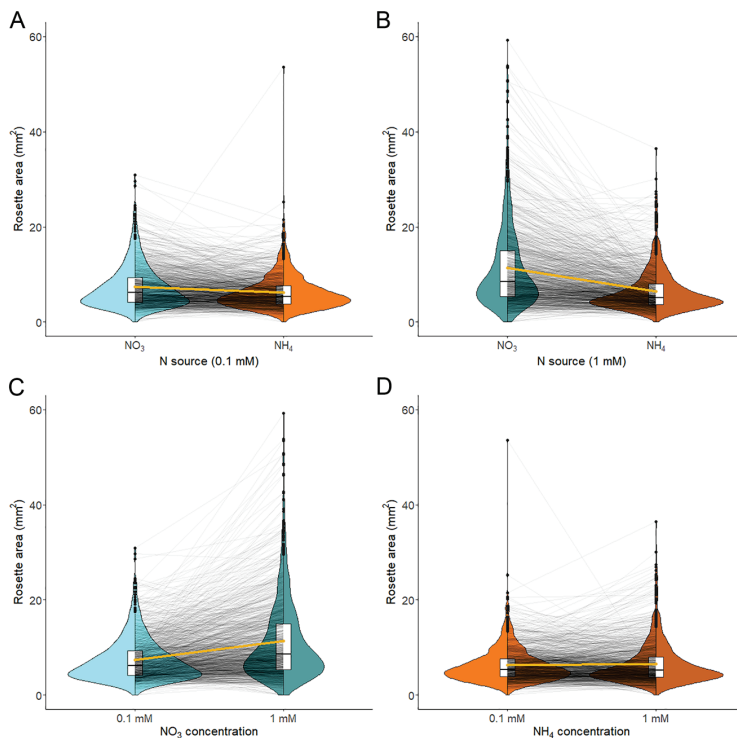


**FIGURE 4** Leaf area of *Arabidopsis* seedlings under different nitrogen nutrition treatments. Black lines connect leaf area of the same accession under different treatments and the gold lines connect the mean for each treatment. Ammonium treatments are indicated in orange and nitrate treatments in blue; lighter shades indicate a concentration of 0.1 mM and darker shades indicate 1 mM. (A) Response to the nitrogen forms at a concentration of 0.1 mM. (B) Response to the nitrogen forms at a concentration of 1 mM. (C) Response to nitrate concentration. (D) Response to ammonium concentration.

and is easily automated, making it suitable for large image sets. The images can be captured and analyzed without the need for specialized imaging equipment or dedicated phenotyping facilities. The agar plate itself can be used as a scale, enabling the analysis of image sets without dedicated two-dimensional scales. With the procedures described here, image sets generated for root phenotyping in other studies might also provide data about shoot phenotypes without much additional effort.

#### AUTHOR CONTRIBUTIONS

J.S. and A.K. wrote the software and performed the validation under supervision from E.K. and A.J.B. E.K. provided resources required to validate this method. A.K. prepared the original draft, and A.J.B. and E.K. edited and revised it. All authors approved the final version of the manuscript.

#### ACKNOWLEDGMENTS

This work was funded in part by USDA-IWYP-16-06702, National Science Foundation grants IOS-16-55810 and CHE-19-04310, and the John B. Orr Endowment.

#### DATA AVAILABILITY STATEMENT

All of the software described in this paper is available on GitHub at <https://github.com/massivejords/Agar-plate-leaf-area>.

#### ORCID

Anna Knapp  <https://orcid.org/0000-0001-7707-9528>  
 Jordan Stefani  <https://orcid.org/0000-0002-2130-536X>  
 Ella Katz  <http://orcid.org/0000-0003-1619-5597>  
 Arnold J. Bloom  <http://orcid.org/0000-0001-6006-1495>

#### REFERENCES

- 1001 Genomes Consortium. 2016. 1,135 genomes reveal the global pattern of polymorphism in *Arabidopsis thaliana*. *Cell* 166(2): 481–491.
- Bloom, A. J. 2015. The increasing importance of distinguishing among plant nitrogen sources. *Current Opinion in Plant Biology* 25: 10–16.
- Easlon, H. M., and A. J. Bloom. 2014. Easy Leaf Area: Automated digital image analysis for rapid and accurate measurement of leaf area. *Applications in Plant Sciences* 2(7): 1400033.
- Gehan, M. A., N. Fahlgren, A. Abbasi, J. C. Berry, S. T. Callen, L. Chavez, A. N. Doust, et al. 2017. PlantCV v2: Image analysis software for high-throughput plant phenotyping. *PeerJ* 5: e4088.
- Katz, E., A. Knapp, M. Lensink, C. K. Keller, J. Stefani, J.-J. Li, E. Shane, et al. 2022. Genetic variation underlying differential ammonium and nitrate responses in *Arabidopsis thaliana*. *The Plant Cell* koac279. <https://doi.org/10.1093/plcell/koac279>
- Kluyver, T., B. Ragan-Kelley, F. Pérez, B. Granger, M. Bussonnier, J. Frederic, K. Kelley, et al. 2016. Jupyter Notebooks—a publishing format for reproducible computational workflows. In F. Loizides and B. Schmidt [eds.], Positioning and power in academic publishing: Players, agents and agendas, 87–90. IOS Press, Amsterdam, the Netherlands.
- Pound, M. P., A. P. French, J. A. Atkinson, D. M. Wells, M. J. Bennett, and T. Pridmore. 2013. RootNav: Navigating images of complex root architectures. *Plant Physiology* 162(4): 1802–1814.

- R Core Team. 2022. R: A language and environment for statistical computing. R Foundation for Statistical Computing, Vienna, Austria. Website: <http://www.R-project.org/> [accessed 10 November 2022].
- Wickham, H. 2016. ggplot2: Elegant graphics for data analysis. Springer, New York, New York, USA.
- Wickham, H., M. Averick, J. Bryan, W. Chang, L. D'Agostino McGowan, R. François, G. Golemund, et al. 2019. Welcome to the Tidyverse. *Journal of Open Source Software* 4(43): 1686.

**How to cite this article:** Knapp, A., J. Stefani, E. Katz, and A. J. Bloom. 2022. Novel method for the quantification of rosette area from images of *Arabidopsis* seedlings grown on agar plates. *Applications in Plant Sciences* 10(6): e11504. <https://doi.org/10.1002/aps3.11504>

## Chapter 2

### **Easy as piads: A low-cost, ultra-high-resolution data acquisition system using a Raspberry Pi**

*(Applications in Plant Sciences, Vol 10, Issue 3. e11485)*

Anna Knapp<sup>1\*</sup>, Arnold J. Bloom<sup>1</sup>

<sup>1</sup>Department of Plant Sciences University of California Davis, One Shields Ave. Davis California 95616 USA.

\*Corresponding author

Author Contribution statement:

A.K. and A.J.B. worked together formulating the idea for the system, A.K. wrote the software, designed the hardware, and tested it under supervision from A.J.B. A.J.B. acquired the funding for the project. A.K. wrote the original draft, and A.J.B. edited and revised it. Both authors approved the final version of the manuscript.

# Easy as piadc: A low-cost, ultra-high-resolution data acquisition system using a Raspberry Pi

Anna Knapp  | Arnold J. Bloom 

Department of Plant Sciences, University of California, Davis, One Shields Avenue, Davis, California 95616, USA

### Correspondence

Anna Knapp, Department of Plant Sciences, University of California, Davis, One Shields Avenue, Davis, California 95616, USA.  
Email: [aknapp@ucdavis.edu](mailto:aknapp@ucdavis.edu)

### Abstract

**Premise:** High-precision data acquisition (DAQ) is essential for developing new methods in the plant sciences. Commercial high-resolution DAQ systems are cost prohibitive, whereas the less expensive systems that are currently available lack the resolution and precision required for many physiological measurements.

**Methods and Results:** We developed the software libraries, called piadc, and hardware design for a DAQ system based on an ultra-high-resolution analog-to-digital converter and a Raspberry Pi computer. We tested the system precision with and without a thermocouple attached and found the precision with the sensor to be better than  $\pm 0.01^\circ\text{C}$  and the maximum possible system resolution to be 0.4 ppm.

**Conclusions:** The ultra-high-resolution DAQ system described here is inexpensive, flexible enough to be used with many different sensors, and can be built by researchers with rudimentary electronic and computer skills. This system is most applicable in the development of new measurement techniques and the improvement of existing methods.

### KEYWORDS

data acquisition, Go, high resolution, Python, Raspberry Pi, thermocouple

Most studies that monitor plants and their environment, whether it be in the field or in the laboratory, require sensors that convert physical or chemical energy into an electrical signal. Some examples of sensors commonly used in plant research are thermocouples, which convert temperature gradients into an electrical potential; photodiodes, which convert light into an electrical current; and strain gauges, which have an electrical resistance that changes when deformed. Many existing methods, such as sap flow measurement (Smith and Allen, 1993), measuring chloroplast movement (Königer et al., 2021), and lysimeters (Payero and Irmak, 2008), utilize these types of sensors, and nearly all methods that use sensors require a data acquisition (DAQ) system to record measurements. Such systems usually have two basic components: (1) an analog-to-digital converter (ADC) that converts the electrical signal from the sensor into digital information and (2) a microcontroller or computer that records and processes

the digital information from the ADC (Emilio, 2013). There are many commercially available DAQ systems, but these products are often expensive and lack flexibility; a project may need a custom DAQ system to overcome these limitations. One ideal choice for a custom system is a Raspberry Pi computer paired with a high-resolution ADC. The low cost, flexibility, and high resolution of such a system is ideal for improving existing plant research methods or for developing new ones.

The Raspberry Pi (<https://www.raspberrypi.org>; Raspberry Pi Foundation, Cambridge, United Kingdom) is an inexpensive, single-board computer that has many easily accessible and configurable input/output (I/O) interfaces, including multiple serial peripheral interfaces (SPI) and general-purpose input/output pins (GPIO), which allow it to be used with a wide variety of ADCs and other peripheral devices. It can run many different operating systems, but the most common is the Linux-based Raspberry Pi OS

This is an open access article under the terms of the Creative Commons Attribution License, which permits use, distribution and reproduction in any medium, provided the original work is properly cited.

© 2022 The Authors. *Applications in Plant Sciences* published by Wiley Periodicals LLC on behalf of Botanical Society of America.

*Appl. Plant Sci.* 2022;10:e11485.

<https://doi.org/10.1002/aps3.11485>

[wileyonlinelibrary.com/journal/AppsPlantSci](https://wileyonlinelibrary.com/journal/AppsPlantSci) | 1 of 6

(<https://www.raspberrypi.org/software/operating-systems/>), which supports most programming languages. The Raspberry Pi and other similar single-board computers have many possible applications in life science research. Its small size and low cost make it suitable for data logging in a variety of environments. The easily accessed I/O interfaces can be connected to many different types of sensors for data acquisition, including cameras for high-throughput plant imaging (Tovar et al., 2018), microphones for bioacoustic data collection (Whytock and Christie, 2017), or gas sensors for air quality monitoring (Suriano, 2021). These same interfaces can also be used to control external components such as mechanical actuators, lighting, or temperature control.

To use sensors for data logging with a Raspberry Pi, an ADC is needed to convert the analog output of a sensor into digital information that the computer can use. Many different ADCs are available for this purpose, and it is important to choose one that is appropriate for the application. A few important specifications to consider when choosing an ADC are bit resolution, sampling rate, and number of channels. There is a necessary tradeoff between an ADC's sampling rate and effective resolution, in that ADCs with very high resolutions are limited to sampling rates in the kilohertz range or less and that as the sampling rate of a given ADC is increased the effective resolution declines (Beev, 2018). For applications where ultra-high-resolution is not critical, there are many ADCs on the market that have readily available open-source software libraries and schematics for interfacing with a Raspberry Pi. For example, Adafruit (<https://www.adafruit.com>; Adafruit Industries, New York, New York, USA) sells ADCs with resolutions ranging from 8- to 16-bits and includes open-source software libraries and hardware design for interfacing them with a Raspberry Pi or other single-board computer. Some sensing applications, however, such as thermocouple psychrometry and load cell measurement, involve the detection

of small changes within a large measurement range. These applications may require higher than 16-bit resolution, thus necessitating an ADC with higher resolution along with low-noise and low-drift electronic components.

The DAQ system described here provides high resolution at a significantly lower cost (around US\$100) than commercial laboratory DAQ systems with similar specifications. It uses the ADS1262 (or ADS1263) ADC (Texas Instruments, Dallas, Texas, USA), which has 32-bit resolution, very low noise and drift (0.16  $\mu$ V peak-to-peak noise and 1 nV/ $^{\circ}$ C offset voltage drift), as well as many built-in features (e.g., 10-channel multiplexer, programmable-gain amplifier, temperature sensor for thermocouple cold junction reference, stable voltage reference, digital filters). The ADS1262 and ADS1263 are identical except that the ADS1263 also includes one additional independently controlled 24-bit ADC. The ADS1262 was used in the system described here, but the ADS1263 can also be used and will perform the same. These features allow this ADC to be used with many different types of sensors; however, the manufacturer of this ADC does not provide a software library that allows it to be easily interfaced with a Linux computer like the Raspberry Pi. To address this, we describe here the open-source software libraries we developed to provide this interface, called piadcs, and the electronic system design required to use this ADC with a Raspberry Pi to make ultra-high-resolution measurements.

## METHODS AND RESULTS

### Basic description

The DAQ system consists of a relatively simple hardware design based around a Raspberry Pi and the ADS1262/3 (Table 1, Figure 1), and the piadcs software libraries

TABLE 1 Materials needed to build the piadcs data acquisition (DAQ) system.

Materials	Purpose	Cost <sup>a</sup>	Supplier(s)
Raspberry Pi 4 Model B	Main computer. Controls and reads data from the ADC. Stores and/or displays output.	\$35–\$75 <sup>b</sup>	Many. See <a href="https://www.raspberrypi.com/products/">https://www.raspberrypi.com/products/</a> for a list of approved suppliers for every region
32-bit ADS1262/3 ADC with breakout board	Converts input voltage into digital information to be read by the Raspberry Pi.	\$30–\$44	ProtoCentral ( <a href="https://protocentral.com">https://protocentral.com</a> ) or, alternatively, Olimex ( <a href="https://www.olimex.com">https://www.olimex.com</a> )
ADuM4151 SPI isolator	Electrically isolates the ADC from the Raspberry Pi. This is important for reducing noise.	\$11	Digi-Key Electronics ( <a href="https://www.digikey.com">https://www.digikey.com</a> ) Mouser Electronics ( <a href="https://www.mouser.com">https://www.mouser.com</a> )
5 V low-dropout (LDO) voltage regulator <sup>c</sup>	Provides stable and low noise 5 V output to the ADC.	\$4–10 <sup>d</sup>	Digi-Key Electronics ( <a href="https://www.digikey.com">https://www.digikey.com</a> ) Mouser Electronics ( <a href="https://www.mouser.com">https://www.mouser.com</a> )
9 V batteries	Power source for the ADC. Batteries are preferable for making low-noise measurements because there is no 60 Hz AC signal to contend with.	\$4	Many

Abbreviations: ADC, analog-to-digital converter; SPI, serial peripheral interface.

<sup>a</sup>Costs are given in U.S. dollars (US\$) at the time of publication.

<sup>b</sup>Varies depending on RAM option selected. The Raspberry Pi 4 Model B comes in 2, 4, and 8 GB RAM options. All three options are appropriate for use in this DAQ system.

<sup>c</sup>There are multiple parts available that could serve this purpose. Examples include MIC2954, MAX883, and  $\mu$ A723. Each of these voltage regulators requires the use of one or more capacitors. Please refer to the datasheet for specific information.

<sup>d</sup>Varies depending on which component is used. Two voltage regulators are required.

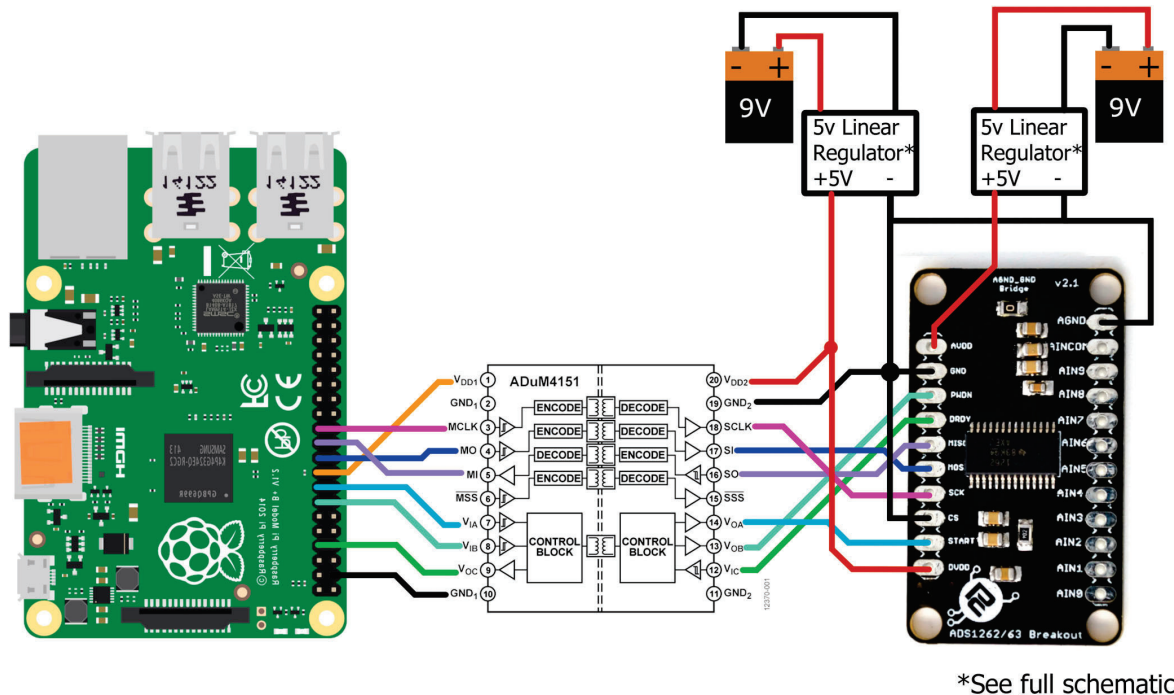


**FIGURE 1** Wiring diagram for the low-cost custom data acquisition (DAQ) system that was used to test the piadcs libraries. The ADS1262 is powered using separate power supplies for the analog and digital components. The analog power supply uses the  $\mu$ A723 150-mA, 40-V, adjustable linear voltage regulator (Texas Instruments), and the digital supply uses the LM10 operational amplifier (Texas Instruments) configured as a voltage regulator. The ADS1262 is connected through a ProtoCentral breakout board (<https://protocentral.com/product/protocentral-ads1262-32-bit-precision-adc-breakout-board/>) and interfaces with a Raspberry Pi 4 Model B through the ADuM4151 7-channel SPI isolator (Analog Devices). Materials to build this DAQ system cost between US\$80 and US\$120 depending on which version of the Raspberry Pi 4 Model B is used. The full schematic, including the power supply circuit, is available on GitHub (<https://github.com/AnnaKnapp/piadcs>).

enable users to easily configure the ADS1262/3 and to collect, convert, and store the output data. The ADS1262/3 is a good choice for a custom DAQ system because of its extremely high (32-bit) resolution and many features that give it flexibility (e.g., a programmable gain amplifier [PGA] with six different gain options, five different digital filters, and a range of 16 possible sampling frequencies from 2.5 to 38,000 samples/second). Functions to modify these settings are found in both piadcs libraries. The libraries also read the ADC output data and convert it into voltage values. There are functions for both reading data continuously or reading on command.

Communication between the Raspberry Pi and the ADS1262/3 uses a combination of SPI and GPIO. The Go version of the library uses the *Periph* library (<https://periph.io>) to control the SPI and GPIO interfaces, and the Python version uses *Spidev* (<https://pypi.org/project/spidev>) and *RPi.GPIO* (<https://pypi.org/project/RPi.GPIO>). There are other ADCs (e.g., ADS1248, ADS1283) on the market that use highly similar programming to the ADS1262/3, and the piadcs libraries are extendable to such ADCs. The libraries also contain documentation and examples that provide a template for programming other ADCs.

## Using the piadcs libraries

There are two functionally equivalent versions of the piadcs library: one is written in Python and the other in Go. The two versions offer different advantages and disadvantages due to differences between the two languages. Python is one of the most widely used programming languages, but as an interpreted language, it runs slower and does not have support for concurrency. Go is less commonly used but still among the top 20 most-used programming languages (TIOBE, 2021). Go is a compiled language, which provides performance advantages over Python and is simpler to read than other compiled languages (e.g., C).

Both versions of the piadcs library are available on GitHub. The Go version can be found at <https://github.com/AnnaKnapp/piadcs> and the Python version at [https://github.com/AnnaKnapp/python\\_piadcs](https://github.com/AnnaKnapp/python_piadcs). Both are installed as packages, and detailed instructions for installation and usage can be found in the README file on GitHub. In brief, the Python library is installed from the command line using the “pip3” command and the Go library is installed using the “go get” command. The “Examples” folders found in the libraries contain code examples showing how to use

the different functions in the library to change ADC settings and collect data from the ADC. Documentation for the Go library can be found at <https://pkg.go.dev/github.com/AnnaKnapp/piadcs> and for the Python library at [https://annaknapp.github.io/python\\_piadcs/](https://annaknapp.github.io/python_piadcs/).

These libraries were designed to run on a Raspberry Pi model 4B or 3B+ running Raspberry Pi OS. It may also be possible to run them on other models provided they are running an up-to-date version of the same operating system, but we have not tested this. There are many helpful guides available on how to get started with a Raspberry Pi and the Raspberry Pi OS. For an official source, the documentation section of the Raspberry Pi website provides a detailed guide (<https://www.raspberrypi.com/documentation/>).

## Hardware design

The DAQ system can be built using the materials listed in Table 1 for about US\$100. The wiring diagram shown in Figure 1 illustrates how the components are connected. The ADS1262/3 can be connected to the Raspberry Pi using one SPI bus and three GPIO pins. In our setup (Figure 1), they are connected via the Raspberry Pi's SPI\_0 and GPIO pins 4, 22, and 27, but any of the available SPI interfaces and GPIO pins could be used. These connections must be specified in the code. Several breakout boards are available for connecting the ADS1262/3 to solderless breadboards for prototyping. A breakout board from ProtoCentral (<https://protocentral.com/product/protocentral-ads1262-32-bit-precision-adc-breakout-board/>; ProtoCentral Electronics, Bengaluru, India) was used in the development of these libraries, but an alternative from Olimex (<https://www.olimex.com>; Olimex, Plovdiv, Bulgaria) would also be suitable (Table 1). A Raspberry Pi-specific

“HAT” for the ADS1263 is available from Waveshare (<https://www.waveshare.com/18983.htm>; Waveshare Electronics, Shenzhen, China). It is compatible with the piadcs libraries, but it is not suitable for low-noise measurements in that one cannot electrically isolate the Raspberry Pi and the ADC because they share the same power supply; moreover, this board situates heat-generating components near the temperature sensor of the ADC.

High-resolution measurements (>18-bits) require low system noise. In our DAQ system, low noise is achieved by electrically isolating the ADS1262/3 from the Raspberry Pi. This requires separate power supplies. The Raspberry Pi is powered by a standard USB-C wall adapter (5.1 V, 3 A), which is usually sold with the computer, whereas the ADS1262/3 is powered by 9-V batteries connected to linear voltage regulators. Batteries are preferable to wall supplies because they do not generate any 60 Hz (or 50 Hz) AC noise. The ADS1262/3 draws less than 6.5 mA, and so a battery lasts for several weeks. The digital communication channels between the ADS1262/3 and the Raspberry Pi are also isolated using the ADuM4151 7-channel SPI isolator (Analog Devices, Wilmington, Massachusetts, USA) (Tsemenko, 2016). All the components for this custom DAQ system can be wired onto a solderless breadboard or made into a printed circuit board. A solderless breadboard setup was used for the test measurement shown in Figure 2.

## System performance

It is possible to make very low noise measurements with this DAQ system as long as the aforementioned electrical considerations are addressed. System performance was tested

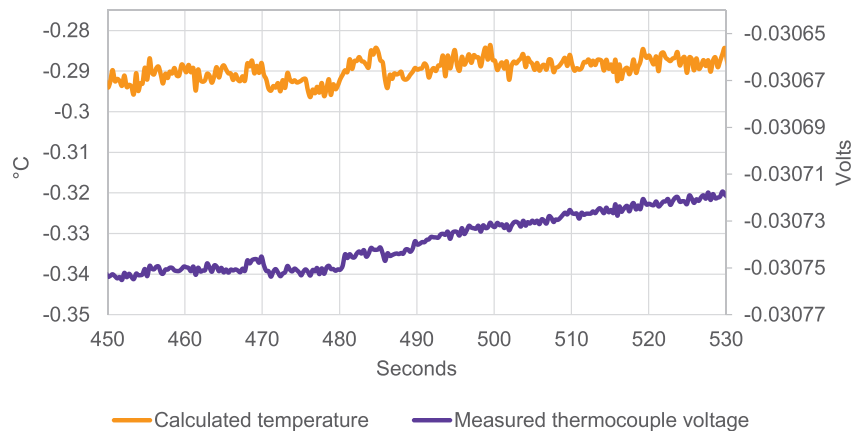


**FIGURE 2** Measurement of a K-type thermocouple in an ice bath using the custom DAQ system shown in Figure 1. The code used to take this measurement was written using the piadcs libraries and can be found in the Examples folder on the piadcs GitHub page as “typeKthermocouple.go” (<https://github.com/AnnaKnapp/piadcs>). The temperature was calculated from the voltage using the K-type thermocouple polynomials provided by the National Institute of Standards and Technology (Garrity, 2000). The temperature sensor built into the ADS1262 was used for cold-junction compensation. The measurement is slightly less than 0°C due to impurities in the water and the rough calibration value that was used to adjust for variation in the thermocouple.

**TABLE 2** Specifications for the custom DAQ system using a Raspberry Pi 4 Model B, the ADS1262/3 analog-to-digital converter (ADC), and the piadcs Go library.

Specification	Typical	Maximum	Unit
Raspberry Pi 4 current draw <sup>a</sup>	600	1200	mA
ADS1262/3 power consumption	25	37	mW
Maximum sampling rate <sup>b</sup>	14,400		sps
Estimated cost of components <sup>c</sup>	\$80–120		USD
	Data rate = 20 sps	Data rate = 7200 sps	
Peak-to-peak noise <sup>d</sup> (PGA set to 1 V/V)	2	60	$\mu$ V
System precision <sup>e</sup> (PGA set to 1 V/V)	0.4	12	ppm
Peak-to-peak noise <sup>f</sup> (PGA set to 32 V/V)	0.125	3.75	$\mu$ V
System precision (PGA set to 32 V/V)	0.8	24	ppm

Abbreviations: PGA, programmable gain amplifier; sps, samples/second.

<sup>a</sup>More information about Raspberry Pi power consumption can be found here <https://www.raspberrypi.org/documentation/hardware/raspberrypi/power/README.md>.

<sup>b</sup>The ADS1262/3 ADCs are capable of higher sampling rates. Rates above 14,400 sps were not achieved in testing with the system described here due to limitations of the current release of the piadcs Go library.

<sup>c</sup>Costs are given in U.S. dollars (USD) at the time of publication.

<sup>d</sup>This does not include sensor noise. It was measured by shorting the analog inputs together. The digital filter was set to Sinc4 for these measurements.

<sup>e</sup>This is calculated by dividing the system noise over the full measurement range.

<sup>f</sup>For comparison, a Campbell Scientific CR3000 (Campbell Scientific, Logan, Utah, USA) has a maximum resolution of 0.67  $\mu$ V and a noise level of about 1.3  $\mu$ V peak to peak ([https://s.campbellsci.com/documents/us/product-brochures/s\\_cr3000.pdf](https://s.campbellsci.com/documents/us/product-brochures/s_cr3000.pdf)). A Measurement Computing MCC134 (Measurement Computing, Norton, Massachusetts, USA) has a temperature noise of 1°C (<https://www.mccdaq.com/PDFs/specs/DS-MCC-134.pdf>).

with and without sensors connected. We first measured baseline system noise with no sensors connected and found that, at slower data rates ( $\leq 20$  samples/second), the system noise is remarkably low (Table 2) and the system has better than 1 ppm precision. As the data rate increases, the noise increases and precision decreases somewhat but is still very good (e.g., at 7200 samples/second, the precision was 12 ppm). The ADS1262/3 has 16 different data rates available ranging from 2.5 to 38,400 samples/second, but our DAQ system only performs well at data rates up to 14,400 samples/second. This is due to a breakdown in serial communication that occurs at higher speeds and could potentially be solved in future releases.

Although the ADC used in this system has a nominal resolution of 32-bits, the actual system precision is lower, especially as the data rate increases. Noise remaining in the system (e.g., thermal noise), along with the inherent tradeoff between ADC speed and resolution, causes the effective resolution of an ADC to be lower than its nominal resolution (Beev, 2018). The noise floor and, therefore, the effective resolution of our system is very close to that specified in the ADS1262 datasheet for the data rates and digital filters tested (Table 2), and is a major improvement over other existing open-source DAQ systems for the Raspberry Pi.

System performance with a connected sensor was tested by measuring the output of a K-type thermocouple submerged in an ice bath using our DAQ system. This setup was able to measure the ice bath temperature with a noise level of less than  $\pm 0.01^\circ\text{C}$  (Figure 2); this was achieved using only the analog front end provided on the ADS1262

with the PGA set to the maximum setting of 32 V/V. An external ultra-low-noise amplifier set to a higher gain could be used instead of the onboard PGA to further decrease noise for applications requiring very low-level measurements (e.g., thermocouple psychrometry).

Our DAQ system has significantly better noise performance than other Raspberry Pi thermocouple DAQ systems. For example, the MCC 134 Thermocouple DAQ HAT for Raspberry Pi (Measurement Computing, Norton, Massachusetts, USA) has greater than 0.5°C measurement error with the same type of thermocouple. This is likely due partly to large thermal gradients caused by placing the DAQ board on top of the heat-generating components of the Raspberry Pi.

## CONCLUSIONS

The greater availability of low-cost, open-source hardware and software makes it more feasible than ever for researchers to develop new methods for measurement and to improve on existing ones. The piadcs libraries and the hardware described here provide a simple and inexpensive way to build a Raspberry Pi-based DAQ system at a much higher resolution than was previously available using existing open-source hardware and software. The libraries contain easy-to-use functions that allow for many different modes of data collection. The wiring shown in the schematic examples can be reproduced easily without extensive equipment or engineering expertise.

The system is flexible and could be used to increase the resolution of existing Raspberry Pi-based systems for monitoring plants and their environment or serve as a substantially lower-cost alternative to expensive laboratory DAQ systems for precision laboratory measurements that necessitate high resolution, low noise, and low temperature drift. Currently, the system is best suited for laboratory applications such as growth chambers and greenhouses. It is compact and could be made portable for use in the field, but the Raspberry Pi's relatively high power consumption makes it unsuitable for long-term data logging where power outlets are not available. Lower-power single-board controllers on the market such as the Raspberry Pi Pico or Arduino (<https://www.arduino.cc/>) could potentially be used for this purpose.

#### AUTHOR CONTRIBUTIONS

A.K. and A.J.B. worked together formulating the idea for the system, A.K. wrote the software, designed the hardware, and tested it under supervision from A.J.B. A.J.B. acquired the funding for the project. A.K. wrote the original draft, and A.J.B. edited and revised it. Both authors approved the final version of the manuscript.

#### ACKNOWLEDGMENTS

This work was funded in part by the U.S. Department of Agriculture (USDA-IWYP-16-06702), the National Science Foundation (grants IOS-16-55810 and CHE-19-04310), and the John B. Orr Endowment. The authors thank Maxime Caly (Doppler, San Francisco, California, USA) for providing expertise on Go.

#### OPEN RESEARCH BADGES



This article has been awarded an Open Materials badge. All materials are publicly accessible via the Open Science Framework at <https://github.com/AnnaKnapp/piadcs> and [https://github.com/AnnaKnapp/python\\_piadcs](https://github.com/AnnaKnapp/python_piadcs). Learn more about the Open Practices badges from the Center for Open Science: <https://osf.io/tyyxz/wiki>.

#### DATA AVAILABILITY STATEMENT

Both versions of the piadcs library, as well as detailed instructions for installation and usage, are available on GitHub

(Go version: <https://github.com/AnnaKnapp/piadcs>; Python version: [https://github.com/AnnaKnapp/python\\_piadcs](https://github.com/AnnaKnapp/python_piadcs)). Documentation for the Go library can be found at <https://pkg.go.dev/github.com/AnnaKnapp/piadcs> and for the Python library at [https://annaknapp.github.io/python\\_piadcs/](https://annaknapp.github.io/python_piadcs/).

#### ORCID

Anna Knapp <http://orcid.org/0000-0001-7707-9528>

Arnold J. Bloom <http://orcid.org/0000-0001-6006-1495>

#### REFERENCES

- Beev, N. 2018. Analog-to-digital conversion beyond 20 bits. Proceedings of the 2018 IEEE International Instrumentation and Measurement Technology Conference (I2MTC), Houston, Texas, USA.
- Emilio, M. D. P. 2013. Data acquisition systems. Springer, New York, New York, USA.
- Garrity, K. 2000. NIST ITS-90 Thermocouple Database - SRD 60. National Institute of Standards and Technology, Gaithersburg, Maryland, USA.
- Königer, M., A. Knapp, L. Futami, and S. Kohler. 2021. Using changes in leaf transmission to investigate chloroplast movement in *Arabidopsis thaliana*. *Journal of Visualized Experiments* 173: e62881.
- Payero, J. O., and S. Irmak. 2008. Construction, installation, and performance of two repacked weighing lysimeters. *Irrigation Science* 26: 191–202.
- Smith, D. M., and S. J. Allen. 1993. Measurement of sap flow in plant stems. *Journal of Experimental Botany* 47(12): 1833–1844.
- Suriano, D. 2021. A portable air quality monitoring unit and a modular, flexible tool for on-field evaluation and calibration of low-cost gas sensors. *HardwareX* 9: e00198.
- TIOBE. 2021. TIOBE index for July 2021 [online]. Website: <https://www.tiobe.com/tiobe-index/> [accessed 9 July 2021].
- Tovar, J. C., J. S. Hoyer, A. Lin, A. Tielking, S. T. Callen, S. E. Castillo, M. Miller, et al. 2018. Raspberry Pi-powered imaging for plant phenotyping. *Applications in Plant Sciences* 6(3): e1031.
- Tsamenko, I. 2016. Texas Instruments ADS1262 32-bit ADC evaluation [online]. Website: [https://xdevs.com/review/ti\\_ads1262\\_p1/](https://xdevs.com/review/ti_ads1262_p1/) [accessed 9 July 2021].
- Whytock, R. C., and J. Christie. 2017. Solo: An open source, customizable and inexpensive audio recorder for bioacoustic research. *Methods in Ecology and Evolution* 8(3): 308–312.

**How to cite this article:** Knapp, A., and A. J. Bloom. 2022. Easy as piadcs: A low-cost, ultra-high-resolution data acquisition system using a Raspberry Pi. *Applications in Plant Sciences* 10(3): e11485. <https://doi.org/10.1002/aps3.11485>

## Chapter 3

### A high-resolution oxygen analyzer using a zirconia sensor

#### 1. Introduction:

Monitoring oxygen and carbon dioxide fluxes from an organism or ecosystem simultaneously can provide a wealth of information about underlying metabolic and geologic processes.

Currently, simultaneous O<sub>2</sub> and CO<sub>2</sub> flux measurements are generally made in organisms or ecosystems where the changes in O<sub>2</sub> concentrations are relatively large compared to the ambient concentration. Common examples include, respirometry in humans (Patel et al., 2023) and other endothermic animals (Hawkes et al., 2014), and in aquatic ecosystems (Vachon et al., 2020).

In the cases of small or ectothermic animals, terrestrial plants, or terrestrial ecosystems, the changes in O<sub>2</sub> concentrations can be small compared to the large ambient oxygen concentration in the atmosphere. For example, typical net CO<sub>2</sub> assimilation per unit leaf area for a plant in ambient conditions is between 600 and 1200  $\mu\text{mol m}^{-2} \text{min}^{-1}$  (Busch, 2022) and photosynthetic O<sub>2</sub> evolution is slightly larger but close in magnitude to CO<sub>2</sub> assimilation. A typical resting O<sub>2</sub> consumption rate for an adult human was found to be around 125  $\mu\text{mol kg}^{-1} \text{min}^{-1}$  (Byrne, 2005) meaning a 70 kg adult may consume more than 9 mmol of O<sub>2</sub> in a minute but a 20 cm<sup>2</sup> *Arabidopsis* plant may produce less than 2  $\mu\text{mol}$  of O<sub>2</sub> over the same time, a difference of nearly 4 orders of magnitude. Measuring these very small O<sub>2</sub> concentration changes requires extremely high-resolution gas analyzers. Here we describe a novel, high-resolution gas-phase oxygen analyzer built using an inexpensive, off-the-shelf zirconia oxygen sensor.

Zirconia oxygen sensors are most frequently used in combustion monitoring applications such as controlling the air-fuel mixtures for gas vehicles, but they have some distinct advantages

that make them of interest for life and environmental science applications. They are robust, inexpensive, and capable of the extremely high precision required to measure photosynthetic oxygen fluxes from terrestrial plants (Bloom et al., 1989). Unlike Clark-style or fuel cell oxygen sensors, Zirconia sensors neither consume oxygen nor deplete a reservoir of chemical reactants and therefore have greater stability over time and a longer service life (Wang et al., 2018).

The sensing element in zirconia oxygen sensors is zirconium dioxide ( $ZrO_2$ ) that becomes a solid oxygen electrolyte at high temperatures (500 °C and above). If different oxygen partial pressures exist on either side of a  $ZrO_2$  cell, it will generate a corresponding Nernst potential (Ramamoorthy et al., 2003). A  $ZrO_2$  cell can also transport oxygen ions from one side to the other when connected to a current source. The most basic implementation of a zirconia oxygen sensor is the potentiometric type which operates by measuring the Nernst potential across a single  $ZrO_2$  cell. Potentiometric sensors require the use of a reference gas on one side of the cell in order to measure the  $O_2$  partial pressure in the sample gas on the other side. In combustion control applications where these sensors are commonly used, the concentration of oxygen is low and high precision is not required. Therefore, the reference gas is often simply atmospheric air.

The requirement for a reference gas can be an impediment for using this type of sensor in applications where higher precision is required, when the  $O_2$  partial pressure in the sample gas is close to that of the atmosphere, and if portability is required. A variety of alternative sensor configurations were developed to eliminate the need for a reference gas including the limiting-current, or amperometric, type (Asada et al., 1990), and the dual-cell combined amperometric and potentiometric type (Maskell, 2000). The dual-cell configuration consists of two  $ZrO_2$  cells separated by a sealed central chamber. One cell, called the pumping cell, is used to pump oxygen in and out of the central chamber and the second, called the sensing cell, is used to measure the

Nernst potential created by the difference in O<sub>2</sub> partial pressure between the central chamber and the external environment. This configuration is of particular interest because there are multiple possible operational modes, some of which have the potential for very high-resolution measurements.

The analyzer described here builds on the “tracking mode” operational method originally described by Benammar and Maskell (1993) in which a sinusoidal current is applied to the pumping cell and a feedback loop is used to keep the average O<sub>2</sub> partial pressure inside the sealed central chamber equal to that in the sample gas being measured. The Nernst potential across the sensing cell has a corresponding sinusoidal component at the same frequency as the pumping current. The amplitude of that sinusoidal component is inversely proportional to the oxygen concentration in the sample gas. The “tracking mode” design was originally intended for combustion monitoring where O<sub>2</sub> concentrations are well below atmospheric and high precision is not required. Our novel design incorporates features, such as a lock-in-amplifier and an ultra-high-resolution analog to digital converter, that improve the signal-to-noise ratio and enable high precision measurements even at atmospheric O<sub>2</sub> concentrations.

## **2. Materials and Methods**

Analyzer design:

The analyzer uses a fast-responding dual-cell zirconia oxygen sensor manufactured by Process Sensing Technologies. A thermocouple probe is fitted into the sensor to enable a PID controller to hold the sensing element at a constant temperature. An analog feedback loop based on the one described by Benammar and Maskell (1993) holds the average O<sub>2</sub> partial pressure inside the sealed central chamber of the sensor at a fixed ratio with that of the external sample gas. A 16-bit

digital-to-analog-converter (DAC) is used to generate a 1 Hz sinusoidal waveform to pump oxygen into and out of the central chamber using the pumping cell. The digital pumping signal is controlled by a custom-built digital lock-in amplifier. The Nernst potential generated across the sensing cell is digitized with a 32-bit analog-to-digital converter. The amplitude and phase of the sense signal is calculated by the lock-in amplifier and a 10-second moving average filter is applied. All software and hardware design files including the full schematics and board files are available in the project github repository (<https://github.com/AnnaKnapp/Zirconia-oxygen-analyzer>) under the CERN Open Hardware License Version 2. A more detailed description of the analyzer design is included in the appendix.

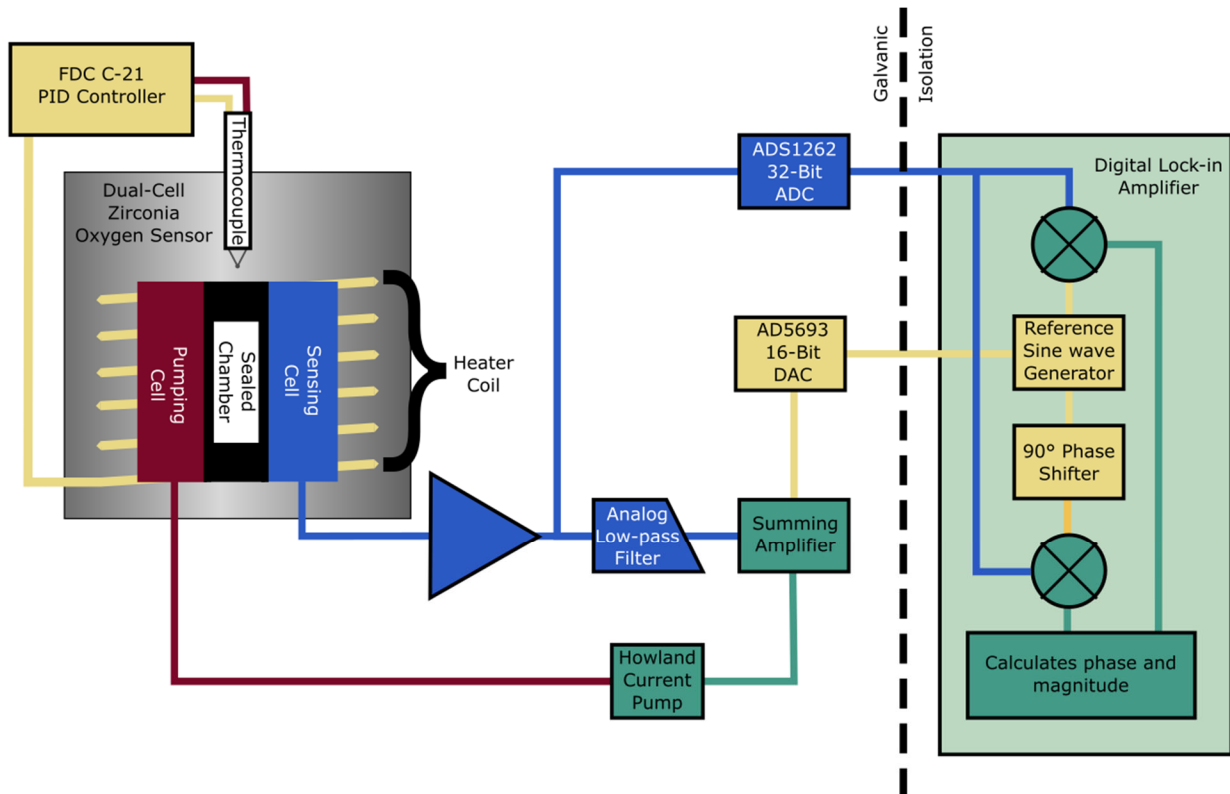


Figure 1. A simplified diagram of the oxygen analyzer.

### Calibration and Characterization:

A gas mixing system was built to mix calibration gasses precisely and control the flow rate of sample gasses to the sensor. High performance Apex MC-Series mass flow controllers (Apex Vacuum LLC) mixed pure oxygen and nitrogen to the desired flow rate and ratio. The outputs of the mass flow controllers were connected to a manifold to ensure consistent mixing. The mass flow controllers were set using Flow Vision MX software (Alicat Scientific). Analyzer response to flow rate was measured by adjusting the flow rate setting in increments of 40 standard cubic centimeters per minute (sccm). A constant flow rate of 200 sccm was used for all other measurements.

Two different calibration gas series were used to assess the analyzer's response for measurements with a large and small range. The oxygen concentrations in the calibration gasses used for large range measurements was 24%, 23%, 22%, 21%, 20%, 19% and 18%, and for small range measurements it was 21.2%, 21.1%, 21.0%, 20.9%, and 20.8%. A one-minute average of the raw analyzer output was taken for each calibration gas, and a calibration curve relating amplitude to oxygen concentration was generated. From these calibration curves, analyzer sensitivity was estimated.

Analyzer repeatability was measured using two different cylinders of compressed air. Tank 1 contained medical compressed air and Tank 2 contained zero air, a synthetic blend of oxygen and nitrogen often used for emissions testing. The reason for this was that the oxygen concentrations in these two tanks would differ by a small but constant amount. Absolute and differential repeatability were measured. Absolute repeatability is defined here as  $1.96 \times \sqrt{2}$  times the standard deviation of the O<sub>2</sub> concentration measured in each tank by the analyzer (Mandel & Lashof, 1987). Differential repeatability refers to  $1.96 \times \sqrt{2}$  times the standard

deviation of the difference in O<sub>2</sub> concentration measured between the two tanks. To obtain a differential repeatability a diverting valve was used to quickly switch between the tanks. Each individual measurement was the average of the measured O<sub>2</sub> concentration over one minute. Analyzer repeatability was assessed in three separate trials conducted on different days. Each trial consisted of 20 separate measurements from each tank.

The temperature at the thermocouple inserted into the sensor was recorded during all measurements including calibration. Temperature sensitivity was measured by adjusting the temperature setpoint on the PID controller in increments of 2 °C and recording the calibrated analyzer output. During these measurements, only air from Tank 1 was used.

### **3. Results and Discussion**

Analyzer calibration and sensitivity:

The amplitude of the Analyzer's output signal was inversely proportional to the oxygen concentration of the sample gas, consistent with the theoretical behavior described by Benammar and Maskell (1993). For the large range calibration (18% - 24% O<sub>2</sub>) a non-linear least squares regression was calculated (Vugrin et al., 2007) giving the relationship  $A = 25.405 \cdot CVO_2 - 0.96$  where A is the amplitude of the output signal in volts and CVO<sub>2</sub> is the volume oxygen concentration of the sample gas in percent. The coefficient of determination for this regression was 0.999995. Because the relationship between oxygen concentration and analyzer output is not linear, the sensitivity also is not constant and will increase as oxygen concentration decreases.

For smaller ranges of oxygen concentration, however, a linear approximation can be used with very good accuracy. For the small range calibration (20.8% - 21.2%) a linear least squares regression was calculated resulting in the relationship  $A = -0.0625 \cdot CVO_2 + 2.68$  with a

coefficient of determination of 0.999517 (Figure 2). Within this range, average sensitivity can be defined as  $-62.5$  mV per percent  $O_2$  or  $-62.5$   $\mu$ V per ppm  $O_2$ . Using a linear fit for calibration would be appropriate when the range of oxygen concentration deviates from ambient by less than  $\pm 2000$  ppm. Terrestrial  $O_2$  concentration change measurements generally fall well within this range (Fassen et al., 2023, Pickers et al., 2016).  $O_2$  concentrations in gas exchange measurements of plants and animals would also usually fall within this range because flow rates are kept high enough to maintain close to ambient atmospheric conditions and prevent condensation of water vapor.

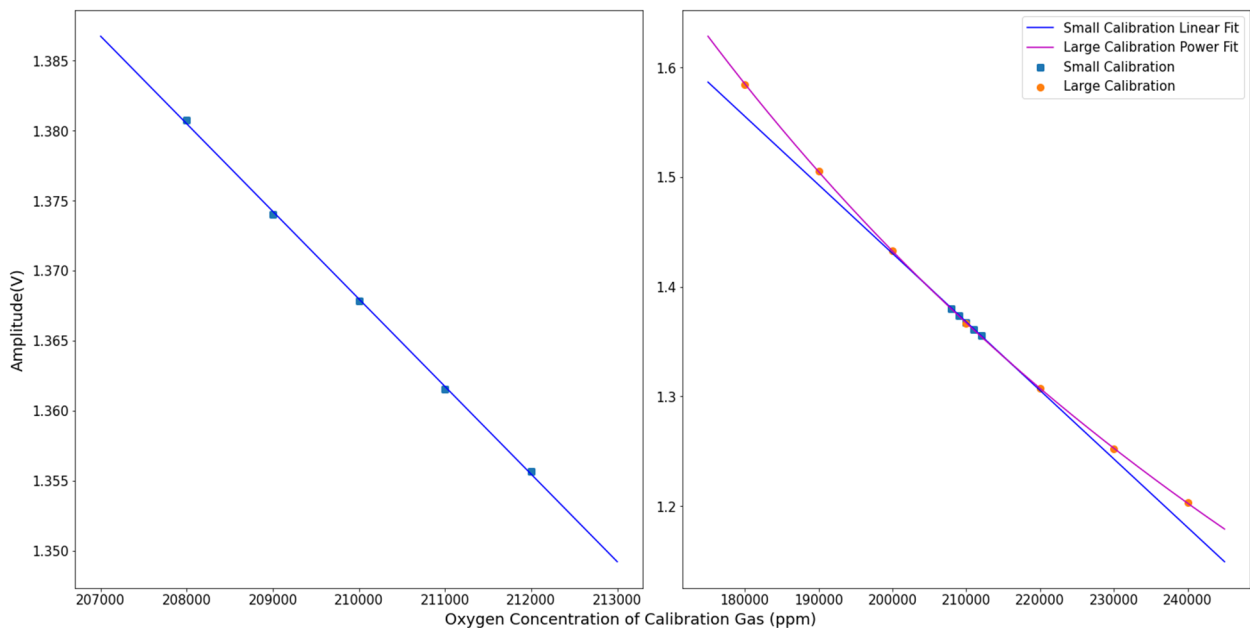


Figure 2. A comparison of analyzer calibration for small and large  $O_2$  concentration ranges. A) A 5-point calibration within the range 20.8% – 21.2% oxygen with a linear fit. B) A 7-point calibration ranging from 18% to 24% with a power fit. The small-range calibration and linear fit are also plotted again for comparison.

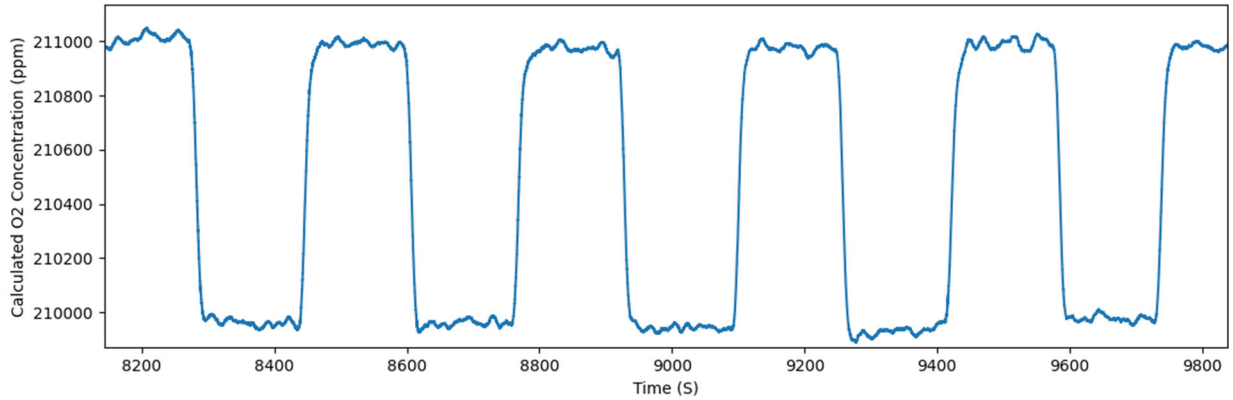


Figure 3. An example trace from the analyzer showing switching between Tank 1 and Tank 2 at 150 second intervals.

Analyzer performance:

The absolute repeatability measurements and the calculated O<sub>2</sub> concentrations of the test tanks differed substantially across the three trials but the differential concentration was more consistent. Analyzer performance was best for differential measurements with a repeatability limit ranging from 55 to 69 ppm while for absolute measurements repeatability ranged from 97 to 213 ppm. The average temperature measured at the thermocouple placed above the sensor was 547.5 °C for trials one and two and 563.0 °C for trial 3. The full results from all three trials are summarized in table 1.

<b>Trial 1 - 547.5 °C</b>	<b>Mean</b>	<b>St. Dev.</b>	<b>Repeatability</b>
Absolute O <sub>2</sub> concentration - Tank 1	21.077 %	73 ppm	202 ppm
Absolute O <sub>2</sub> Concentration - Tank 2	21.182 %	77 ppm	213 ppm
Differential O <sub>2</sub> Concentration (Tank 2 - Tank 1)	1052 ppm	25 ppm	69 ppm

<b>Trial 2 - 547.5 °C</b>			
Absolute O <sub>2</sub> concentration - Tank 1	20.993 %	38 ppm	105 ppm
Absolute O <sub>2</sub> Concentration - Tank 2	21.975 %	35 ppm	97 ppm
Differential O <sub>2</sub> Concentration (Tank 2 - Tank 1)	1045 ppm	25 ppm	69 ppm
<b>Trial 3 - 563.0 °C</b>			
Absolute O <sub>2</sub> concentration - Tank 1	21.026 %	47 ppm	130 ppm
Absolute O <sub>2</sub> Concentration - Tank 2	21.127 %	48 ppm	133 ppm
Differential O <sub>2</sub> Concentration (Tank 2 - Tank 1)	1010 ppm	20 ppm	55 ppm

Table 1. Summary of analyzer performance over three trials.

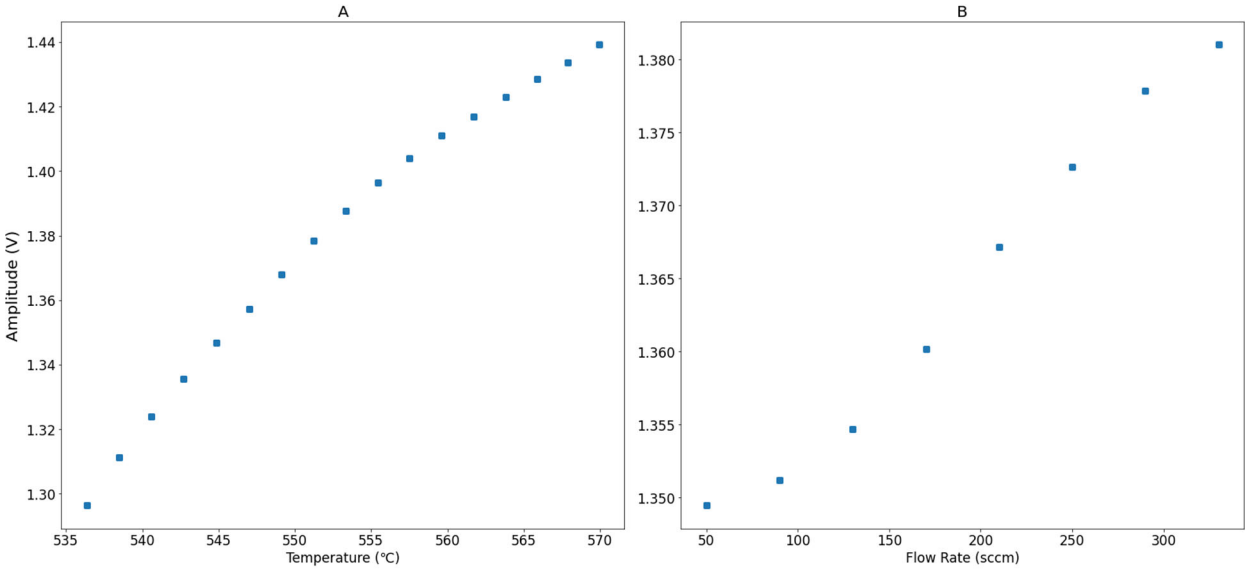


Figure 4. Analyzer response to temperature and flow rate. A) Raw amplitude output of the analyzer measured at temperature intervals of 2 °C from 536 °C to 570 °C. B) Raw amplitude output of the analyzer measured at flow rate intervals of 40 sscm from 50 to 330 sscm.

Temperature and Flow Rate sensitivity:

The average sensitivity of the analyzer to flow rate was 0.12 mV per sscm and therefore flow rate would need to be controlled with a repeatability of better than 0.5 sscm to achieve a O<sub>2</sub> measurement precision of 1 ppm. The specified repeatability limit of the mass flow controller used to test the analyzer was 0.4 sscm at the flow rate used for all measurements and therefore did not substantially limit O<sub>2</sub> concentration measurement repeatability.

The average temperature sensitivity of the analyzer for the range 536 °C to 570 °C was 4.2 mV per degree. It is important to note that this temperature was measured from right above the sensing element and not from inside the heating coil, so the true temperature of the sensing element was likely higher. The response to temperature was nonlinear and temperature sensitivity decreases somewhat at higher temperatures.

Temperature control is extremely critical for high precision measurements and this analyzer design has a very high temperature sensitivity. Given the analyzers sensitivities of -62.5 μV per ppm O<sub>2</sub> and 4.2 mV per degree, the temperature of the sensing element would theoretically need to be held at a constant temperature with a stability better than ± 0.015 °C to achieve an oxygen measurement repeatability of ± 1 ppm. During the three trials used to assess the repeatability of oxygen measurements, the repeatability of the temperature measured at the thermocouple ranged from 0.04 to 0.06 °C indicating that temperature control could be a limiting factor in achieving higher O<sub>2</sub> measurement precision. Temperature variation was often correlated to variations in the measured O<sub>2</sub> concentration indicating that temperature instability could limit O<sub>2</sub> precision to an even greater degree than predicted by the calculated sensitivities alone (Figure 5).

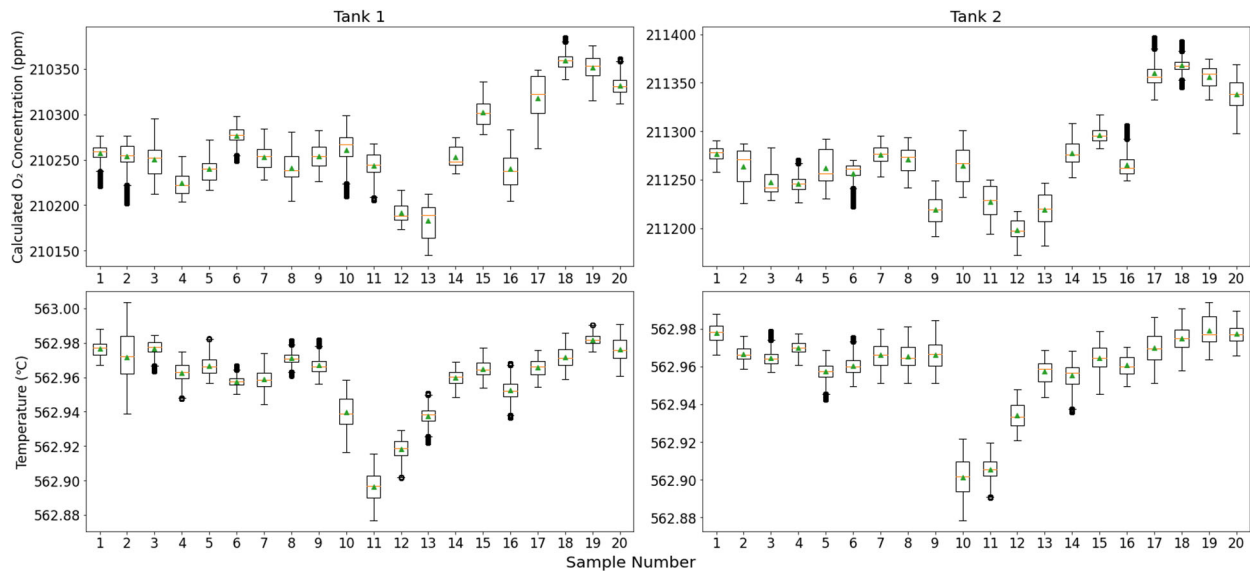


Figure 5. Comparison of O<sub>2</sub> measurement and analyzer temperature during trial 3. The calculated O<sub>2</sub> concentration for 20 consecutive measurements of tank 1 and tank 2 are plotted on the top left and right respectively. The temperatures measured at the thermocouple placed directly above the oxygen sensor during each measurement are plotted on the bottom underneath their corresponding O<sub>2</sub> measurement.

#### 4. Limitations and Future Directions

The temperature readings obtained in our experiments likely do not accurately capture the true temperature of the zirconia sensing element due to the placement of the temperature sensor outside of the heater coil. An integrated temperature sensor is needed to accurately assess the temperature response of the system and determine the extent to which temperature instability limits the analyzers performance. Temperature control could also be improved with better temperature sensor placement because it would allow the controller to respond faster to temperature changes at the sensing element. There are currently no commercially available sealed dual-cell zirconia O<sub>2</sub> sensors with an integrated temperature sensor so a custom sensor

would need to be fabricated. Alternatively, a soft sensing approach could be used to more accurately estimate the temperature of the sensing element. Such an approach could use additional sensors placed at different parts of the system. For example, flow and temperature sensors could be placed along the incoming gas stream, and a model-based control algorithm could be used to predict how those changes will impact the temperature of the sensing element and pre-emptively adjust the heater before any change is registered on the thermocouple placed above the sensor. Temperature control of the incoming gas stream and of other electrical components could also potentially improve performance.

Many configurations and operational modes of zirconia-based oxygen sensors have not yet been investigated for their potential to make the high precision measurements. A second operational mode for dual-cell zirconia sensors was developed by Benammar and Maskell (1994) that also has the potential to make very high-resolution measurements. This alternative method is leakage tolerant and may work well at higher frequencies improving the noise reduction from a lock-in-amplifier. Limiting current type zirconia O<sub>2</sub> sensors have a lower temperature sensitivity and can be operated at lower temperatures (Saji, 1987) making them of interest for developing high resolution O<sub>2</sub> analyzers.

## **5. Conclusion**

With a novel oxygen analyzer design, we have demonstrated the feasibility of using dual-cell zirconia oxygen sensors for very high precision measurements. The differential measurement repeatability of our analyzer at ambient O<sub>2</sub> concentrations is nearly two orders of magnitude greater than the manufacturer supplied analyzer for the sensor used (SST sensing, 2016). The design is also open source and can be constructed from inexpensive off-the-shelf components.

Our design has a small form factor and relatively low power consumption (< 10 W) making it suitable for use in the field. In its current iteration, it is not yet suitable for measuring photosynthetic O<sub>2</sub> fluxes, however it could be used for applications with larger O<sub>2</sub> fluxes such as respirometry. Improvements to the sensor temperature measurement and control have the potential to further improve the analyzer's performance.

## 6. References

- Asada, A., Yamamoto, H., Nakazawa, M., & Osanai, H. (1990). Limiting current type of oxygen sensor with high performance. *Sensors and Actuators B: Chemical*, 1(1–6), 312–318. [https://doi.org/10.1016/0925-4005\(90\)80222-1](https://doi.org/10.1016/0925-4005(90)80222-1)
- Benammar, M., & Maskell, W. C. (1993). Measurement of oxygen partial pressure using fully-sealed zirconia pump—gauge devices operated in the tracking mode. Part 2. *Sensors and Actuators B: Chemical*, 15(1–3), 162–165. [https://doi.org/10.1016/0925-4005\(93\)85043-a](https://doi.org/10.1016/0925-4005(93)85043-a)
- Benammar, M., & Maskell, W. C. (1994). A leakage-tolerant zirconia pump-gauge oxygen sensor. *Measurement Science and Technology*, 5(12), 1566–1571. <https://doi.org/10.1088/0957-0233/5/12/020>
- Bloom, A. J., Caldwell, R. M., Finazzo, J., Warner, R. L., Weissbart, J. (1989). Oxygen and carbon dioxide fluxes from barley shoots depend on nitrate assimilation. *Plant Physiology*, 91(1), 352–356, <https://doi.org/10.1104/pp.91.1.352>
- Busch, F. A., Ainsworth, E. A., Amtmann, A., Cavanagh, A. P., Driever, S. M., Ferguson, J. N., Kromdijk, J., Lawson, T., Leakey, A. D., Matthews, J. S., Meacham-Hensold, K., Vath, R. L., Vialet-Chabrand, S., Walker, B. J., & Papanatsiou, M. (2024). A guide to photosynthetic gas exchange measurements: Fundamental principles, best practice and potential pitfalls. *Plant, Cell & Environment*, 47(9), 3344–3364. <https://doi.org/10.1111/pce.14815>
- Byrne, N. M., Hills, A. P., Hunter, G. R., Weinsier, R. L., & Schutz, Y. (2005). Metabolic equivalent: One size does not fit all. *Journal of Applied Physiology*, 99(3), 1112–1119. <https://doi.org/10.1152/jappphysiol.00023.2004>
- Faassen, K. A., Nguyen, L. N., Broekema, E. R., Kers, B. A., Mammarella, I., Vesala, T., Pickers, P. A., Manning, A. C., Vilà-Guerau de Arellano, J., Meijer, H. A., Peters, W., & Lujckx, I. T. (2023). Diurnal variability of atmospheric O<sub>2</sub>, CO<sub>2</sub>, and their exchange ratio above a boreal forest in southern Finland. *Atmospheric Chemistry and Physics*, 23(2), 851–876. <https://doi.org/10.5194/acp-23-851-2023>

Hawkes, L. A., Butler, P. J., Frappell, P. B., Meir, J. U., Milsom, W. K., Scott, G. R., & Bishop, C. M. (2014). Maximum running speed of captive bar-headed geese is unaffected by severe hypoxia. *PLoS ONE*, 9(4). <https://doi.org/10.1371/journal.pone.0094015>

Mandel, J., & Lashof, T. W. (1987). The nature of repeatability and reproducibility. *Journal of Quality Technology*, 19(1), 29–36. <https://doi.org/10.1080/00224065.1987.11979030>

Maskell, W. (2000). Progress in the development of Zirconia Gas Sensors. *Solid State Ionics*, 134(1–2), 43–50. [https://doi.org/10.1016/s0167-2738\(00\)00712-8](https://doi.org/10.1016/s0167-2738(00)00712-8)

Pickers, P. A., Manning, A. C., Sturges, W. T., Le Quéré, C., Mikaloff Fletcher, S. E., Wilson, P. A., & Etchells, A. J. (2017). In situ measurements of atmospheric O<sub>2</sub> and CO<sub>2</sub> reveal an unexpected O<sub>2</sub> signal over the tropical Atlantic Ocean. *Global Biogeochemical Cycles*, 31(8), 1289–1305. <https://doi.org/10.1002/2017gb005631>

SST Sensing. (2016) OXY-LC Oxygen Sensor Interface Board. DS-0058 REV 6.

Patel H., Kerndt C. C., Bhardwaj A. (2023) Physiology, Respiratory Quotient. *StatPearls*.

Ramamoorthy, R., Dutta, P.K. & Akbar, S.A. (2003). Oxygen sensors: Materials, methods, designs and applications. *Journal of Materials Science* 38, 4271–4282 <https://doi.org/10.1023/>

Saji, K. (1987). Characteristics of limiting current-type oxygen sensor. *Journal of The Electrochemical Society*, 134(10), 2430–2435. <https://doi.org/10.1149/1.2100216>

Vachon, D., Sadro, S., Bogard, M. J., Lapierre, J., Baulch, H. M., Rusak, J. A., Denfeld, B. A., Laas, A., Klaus, M., Karlsson, J., Weyhenmeyer, G. A., & del Giorgio, P. A. (2020). Paired O<sub>2</sub>–CO<sub>2</sub> measurements provide emergent insights into aquatic ecosystem function. *Limnology and Oceanography Letters*, 5(4), 287–294. <https://doi.org/10.1002/lol2.10135>

Vugrin, K. W., Swiler, L. P., Roberts, R. M., Stucky-Mack, N. J., & Sullivan, S. P. (2007). Confidence region estimation techniques for nonlinear regression in groundwater flow: Three case studies. *Water Resources Research*, 43(3). <https://doi.org/10.1029/2005wr004804>

Q. Wang, Jia-Ming Zhang & Shuai Li (2019) Minreview: Recent advances in the development of gaseous and dissolved oxygen sensors, *Instrumentation Science & Technology*, 47:1, 19-50, DOI: 10.1080/10739149.2018.1453835

## Conclusion and future directions

The three tools described here have applications beyond the original research question they were designed to solve. The rosette area measurement software could be used in any studies involving *Arabidopsis* grown on agar plates. The high-resolution data acquisition system can be applied to any research where high resolution is required, from plant sciences applications like sap flow and psychrometry measurements to fields outside of life sciences. The O<sub>2</sub> analyzer does not yet have the level of precision required to measure photosynthetic O<sub>2</sub> fluxes but the potential exists for future improvements. In its current state it could be used for applications like respirometry where the O<sub>2</sub> fluxes are somewhat larger.

Chapter 1 described an automated tool to measure the rosette area of *Arabidopsis* seedlings grown on agar plates. We demonstrated that the agar plate itself can be reliably used as a scale when no other 2-D scale indicators are provided. The rosette area measurements for seedlings on agar plates had good agreement with the same rosettes photographed from directly above after excision from the plate indicating that even though rosettes are somewhat askew, leaf area can still be measured. This tool was then used to quickly measure rosette area from more than 2000 plate images with minimal human intervention. The rosette area phenotype data generated from this was used in a larger study of the genetic basis of response to different nitrogen forms and concentrations in more than 1000 *Arabidopsis* accessions. *Arabidopsis* seedlings grown on agar plates are commonly photographed for quantification of root traits. Our tool provides an automated way to simultaneously quantify shoot traits in these studies.

The data acquisition system described in chapter 2 came about as part of the development of the high precision O<sub>2</sub> analyzer described in chapter 3 but was designed to be general-purpose. Our design provides simple hardware and software interfaces between a raspberry pi and an ultra-high-precision ADC with 32-bits of resolution. We demonstrated the use of this system with a thermocouple for very high-resolution temperature measurements but almost any type of sensor could be compatible with it. The software libraries for this project have received 18 stars on github so far indicating that there is interest in the project. I have also received personal correspondence from four different individuals who have been using our data acquisition system for applications ranging from geophysics to semiconductor research. Because of the interest this project has received there is an opportunity to add more features to the software libraries and further develop the open-source hardware further into a single printed circuit board that would further simplify the use of the system.

Chapter 3 described a novel O<sub>2</sub> analyzer capable of very high precision that can be built with relatively inexpensive off-the-shelf components. Its design is fairly simple and can be built with a small form factor making it suitable for use inside and outside of the laboratory. The O<sub>2</sub> concentration measurement repeatability achieved by this analyzer in differential mode was better than 70 ppm against an O<sub>2</sub> background of 21%. This is not quite precise enough for the original intended application of measuring photosynthetic O<sub>2</sub> fluxes, but it indicates good progress towards achieving that goal. It still could be used for applications like respirometry in animals where fluxes of O<sub>2</sub> are larger, or in situations where the background concentration of O<sub>2</sub> is smaller. We found that temperature instability was likely a major limiting factor in the analyzer's performance. Future improvements of the temperature measurement and control could improve the precision, increasing the number of possible applications. The design of the analyzer

is novel, and its high performance proves the viability of zirconia sensors for very high precision measurements. Further investigation into different zirconia sensor configurations and operational modes is warranted.

## **Appendix – Detailed oxygen analyzer design description and supplemental figures**

### **Detailed description of the oxygen analyzer:**

#### Oxygen sensor and temperature control

The analyzer uses a O<sub>2</sub>S-FR-T4-5P zirconia O<sub>2</sub> sensor produced by Process Sensing Technologies. Temperature control of the sensor was required for high precision measurements. The sensor does not have an integrated temperature sensor, so it was modified to accommodate one. A hole was cut using a lathe into the top of the sensor cover to fit a 1/16 inch ceramic insulated K-type thermocouple probe (Omega). A mounting block was machined out of a PEEK plastic cube to hold the thermocouple and sensor in place and allow the sample gas to flow across the sensor. The sensor temperature was controlled using a C21 PID controller (Future Design Controls) to adjust the voltage supplied to the sensor's internal heating coil.

#### Control loop and oxygen pump:

An analog control loop provides the feedback loop that holds the average O<sub>2</sub> partial pressure inside the sealed central chamber of the sensor ( $P_1$ ) at a fixed ratio with that of the external sample gas ( $P_E$ ). A 16-bit Digital-to-analog-converter (DAC) controlled by an M4 Grand Central microcontroller (Adafruit) is used to generate a 1 Hz sinusoidal waveform to pump oxygen into and out of the central chamber.

The sensing cell's corresponding 1 Hz sinusoidal output is amplified by an AD8429 instrumentation amplifier and offset by  $-2.5V$ . The amplified and offset sense signal is then filtered using a second order active lowpass filter designed to remove the pumping frequency and isolate the average Nernst potential. This filtered signal is used to offset the 1 Hz sinusoidal waveform generated by the DAC via a summing amplifier. The offset waveform drives a Howland current pump to generate a sinusoidal current that keeps the average  $P_E : P_I$  ratio constant and pumps a constant amount of oxygen into and out of the central chamber each cycle. The offset of  $-2.5V$  with an amplifier gain of 50 keeps the sensor's average Nernst potential at 50mV, corresponding to a  $P_E : P_I$  ratio of about 13.

This offset was not present in the analyzer design described by Bennamar and Maskell but was added here to improve the sensor's performance at higher  $O_2$  concentrations than those in the original application. Forcing  $P_I$  to stay relatively small with this offset increases the amplitude of the signal due to the larger relative amount of oxygen pumped in and out each cycle. The full schematic for the analog control loop is provided in Figure A-1. Full analog control loop schematic is shown in figure A-1 and the PCB built from that schematic is shown in figure A-2.

Data acquisition and lock-in-amplifier:

A custom digital lock-in amplifier (LIA) was built for the analyzer to improve noise performance. LIAs are able to isolate a signal of interest from other unwanted noise frequencies by multiplying the signal of interest with a frequency matched reference signal. In the case of this  $O_2$  analyzer the reference signal is the 1 Hz sine wave generated by the 16-bit DAC, and the signal of interest is the sense signal generated by the sensor which is also a 1 Hz sine wave.

The amplified sense signal is filtered with a second order analog bandpass filter and digitized using the ADS1262 32-bit analog to digital converter (ADC) controlled by the adafruit M4 microcontroller. The ADC and DAC were synchronized by the microcontroller to update at a frequency of 500 samples per second. The temperature at the thermocouple placed just above the oxygen sensor is also measured and recorded. The thermocouple signal was amplified by a thermocouple amplifier with built-in cold junction compensation (Adafruit Inc). The amplified signal was then digitized by a second ADS1262 32-bit ADC

The microcontroller passes the digitized sense signal, thermocouple signal, and the index value of the lookup table used to generate the reference sinusoid to a PC via a USB cable. The PC ran a python script that calculates the amplitude and phase of the sense signal along with the temperature at the thermocouple. To account for any phase shift between the signal and reference the signal is also multiplied by the reference shifted by  $90^\circ$ . The resulting amplitude and phase values are passed through a 10-second moving average filter. A diagram of the LIA architecture is shown in figure A-3.

A GUI on the laptop graphed raw sense and reference signals, the output of the lock in amplifier, and the temperature in real time (Figure A-4). These data were also recorded to a text file.

### Power supplies and isolation

Because of the very high resolution measurements required, extra steps were taken to reduce noise as much as possible. The analog portion of the data acquisition system was powered using a low noise power supply consisting of two rechargeable 9V batteries (EBL). LM1084 and

LM2990 low-dropout voltage regulators (Texas Instruments) were used to generate +5 V and – 5 V sources respectively.

The digital communication interfaces of the ADCs and DAC were both galvanically isolated to prevent noise from digital switching from interfering with the signal being measured. ADuM4151 SPIisolator™ digital isolators (Analog Devices) provided isolation between the ADS1263 ADCs and the microcontroller. An Adafruit ISO1540 Bidirectional I2C Isolator breakout board (Adafruit Inc.) isolated the 16-bit DAC from the microcontroller. Additionally a USB isolator (Adafruit Inc.) was used to isolate the microcontroller from the laptop.



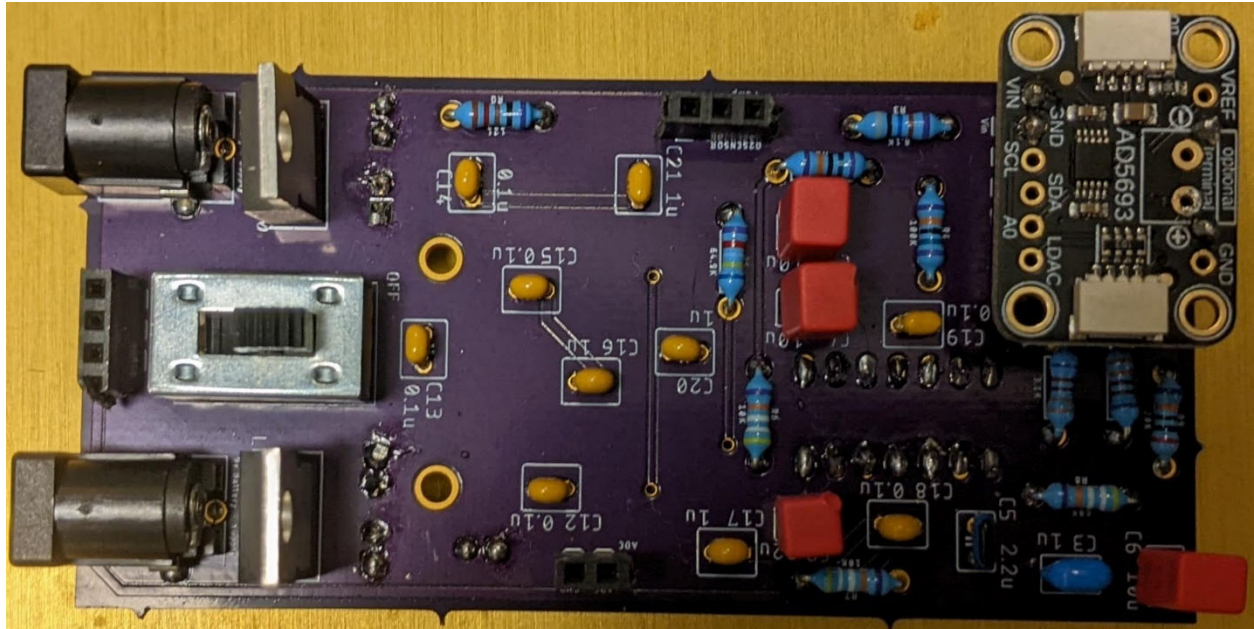


Figure A-2. PCB that was used in the analyzer. Contains the analog control loop circuitry shown in figure A-1. The 16-bit DAC (top right corner) is also mounted onto the board.

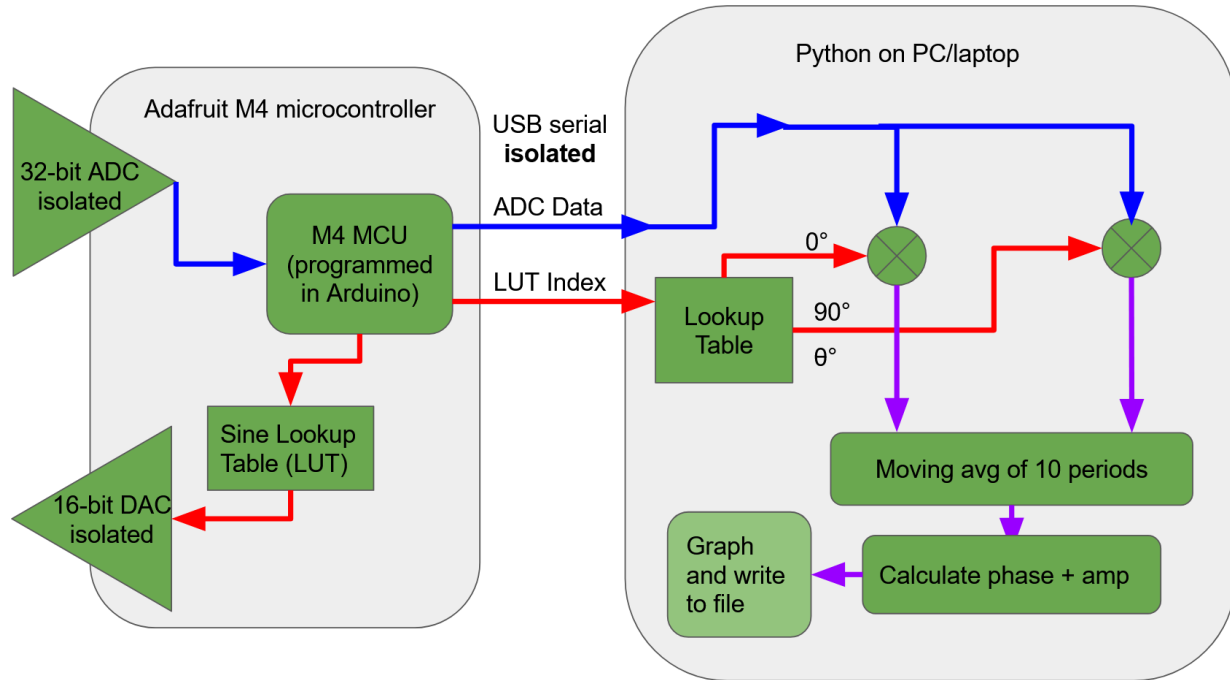


Figure A-3. Diagram showing the overall architecture of the lock-in-amplifier used in the O<sub>2</sub> analyzer.

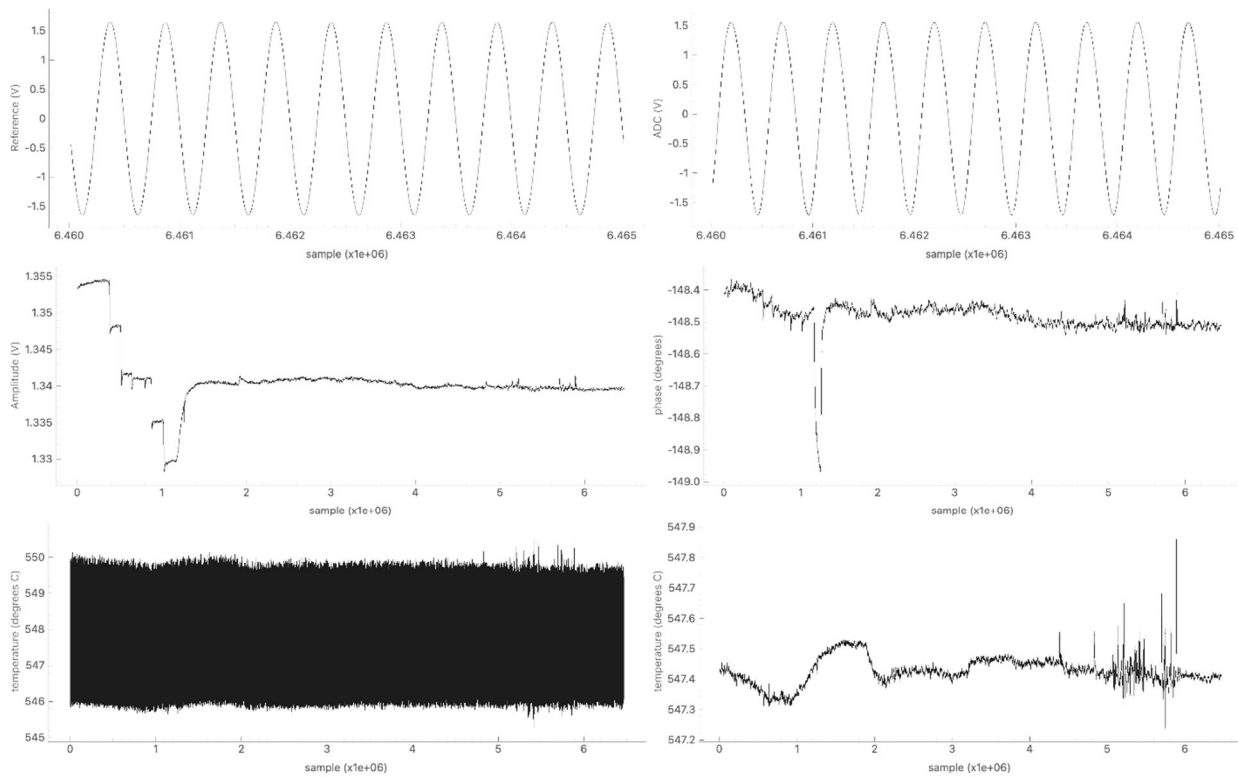


Figure A-4. Example screenshot of the GUI used to plot data from the analyzer in real-time as measurements are being collected. This particular screenshot shows a 5-point calibration followed by a long hold at a constant O<sub>2</sub> concentration. Top graphs show the sense (left) and reference (right) signal plotted over 10 seconds. Middle graphs are the raw amplitude (left) and phase (right) output of the sense signal from the beginning of the measurement. Bottom left is the temperature measured at the thermocouple placed directly above the analyzer from the beginning of the measurement. Bottom right is the same data as on the bottom left except a 10-second moving average filter has been applied.